

1 **Nonlinear responses of particulate nitrate to NO_x emission controls in**
2 **the megalopolises of China**

3 Mengmeng Li^{1,*}, Zihan Zhang¹, Quan Yao², Tijian Wang¹, Min Xie¹, Shu Li¹,
4 Bingliang Zhuang¹ and Yong Han³

5 ¹ School of Atmospheric Sciences, Nanjing University, Nanjing 210023, China

6 ² Statistical Bureau for the Qingjiangpu District, Huaian 223001, China

7 ³ Guangdong Province Key Laboratory for Climate Change and Natural Disaster
8 Studies, School of Atmospheric Sciences, Sun Yat-Sen University, Guangzhou
9 510000, China

10 * Corresponding author: mengmengli2015@nju.edu.cn

11 **Abstract**

12 Nitrate is an increasingly important component of fine particulate matter (PM_{2.5})
13 in Chinese cities. The production of nitrate is not only related to the abundance of its
14 precursor but also supported by the atmospheric photochemical oxidants, raising a
15 new challenge to the current emission control actions in China. This paper uses
16 comprehensive measurements and a regional meteorology-chemistry model with
17 optimized mechanisms to establish the nonlinear responses between particulate nitrate
18 and nitrogen oxides (NO_x) emission controls in the megalopolises of China. Nitrate is
19 an essential component of PM_{2.5} in eastern China, accounting for 9.4–15.5% and
20 11.5–32.1% of the PM_{2.5} mass for the warm and cold seasons. The hypothetical NO_x
21 emission reduction scenarios (–10%~–80%) during summer-autumn result in almost
22 linearly lower PM_{2.5} by –2.2% in Beijing-Tianjin-Hebei (BTH) and –2.9% in Yangtze
23 River Delta (YRD) per 10% cut of NO_x emissions, whereas they lead to a rather
24 complicated response of PM components in winter. Wintertime nitrate is found to
25 increase by +4.1% in BTH and +5.1% in YRD per 10% cut of NO_x emissions, with

26 nearly unchanged nitric acid (HNO_3) and higher dinitrogen pentoxide (N_2O_5)
27 intermediate products produced from the increased atmospheric oxidants levels. An
28 inflexion point appears at 40–50% NO_x emission reduction, and a further cut in NO_x
29 emissions is predicted to cause –10.5% reduction of nitrate for BTH and –7.7% for
30 YRD per 10% cut of NO_x emissions. In addition, the 2012–2016 NO_x control strategy
31 actually leads to no changes or even increases of nitrate in some areas (8.8% in BTH
32 and 14.4% in YRD) during winter. Our results also emphasize that ammonia (NH_3)
33 and volatile organic compounds (VOC_s) are effective in controlling nitrate pollution,
34 whereas decreasing the sulfur dioxide (SO_2) and NO_x emissions may have counter-
35 intuitive effects on nitrate aerosols. This paper helps understand the nonlinear aerosol
36 and photochemistry feedbacks, and defines the effectiveness of proposed mitigations
37 for the increasingly serious nitrate pollution in China.

38

39 **1 Introduction**

40 Secondary inorganic aerosols (SIA), including sulfate (SO_4^{2-}), nitrate (NO_3^-) and
41 ammonium (NH_4^+) account for 30–60% of the total fine particulate matter ($\text{PM}_{2.5}$)
42 mass during haze events in China (Huang et al., 2014a; Zhao et al., 2013). Since the
43 enactment of the Air Pollution Action Plan in 2013, the Chinese government has
44 taken drastic measures to reduce the emissions of sulfur dioxide (SO_2), nitrogen
45 oxides (NO_x) and primary $\text{PM}_{2.5}$, leading to significant decreases in sulfate and
46 overall $\text{PM}_{2.5}$ concentrations in cities (Silver et al., 2018; Li et al., 2021a; Wang et al.,
47 2017b). Meanwhile, the nitrogen/sulfur (N/S) ratio in $\text{PM}_{2.5}$ increased significantly
48 and nitrate had been the main component of $\text{PM}_{2.5}$ (16–45%) during haze episodes,
49 despite a more than 20% reduction in the concentrations of its precursor NO_x (Shao et
50 al., 2018; Wen et al., 2018; Zhai et al., 2019). The increasingly serious nitrate
51 pollution has emerged to be the new emphasis of air pollution controls in China.

52 Nitrate formation involves complex multiphase chemical reactions. In the
53 daytime, nitrogen dioxide (NO_2) reacts with hydroxyl radical (OH) to produce nitric
54 acid (HNO_3). With excess ammonium (NH_3), low temperature and insufficient
55 sulphuric acid, this reaction can proceed quickly and produce high ammonium nitrate
56 (Seinfeld and Pandis, 2006). In the nighttime, however, high-concentration NO_2 reacts
57 with ozone (O_3) to produce the nitrate radical (NO_3) and dinitrogen pentoxide (N_2O_5).
58 The heterogeneous hydrolysis of N_2O_5 on wet particles is the main pathway for
59 nocturnal nitrate formation (56–97%) (He et al., 2018; Pathak et al., 2011; Xue et al.,
60 2014).

61 Nitrate chemistry is not only related to the abundance of its precursor NO_x , but
62 also supported by the atmospheric oxidants (e.g., OH and O_3) produced from the
63 photochemical reactions of NO_x and volatile organic compounds (VOCs) (Meng et al.,

64 1997). Using a box model, some studies have determined that the relationship
65 between particulate nitrate and NO_x emissions is nonlinear depending on the ozone
66 chemical sensitivity regime (Pun and Seigneur, 2001; Nguyen and Dabdub, 2002).
67 Pun and Seigneur (2001) showed that the daytime HNO_3 production was more
68 sensitive to the concentrations of atmospheric oxidants, and that in the VOC-limited
69 regime the decrease of HNO_3 production due to the NO_x emission control might be
70 offset by the increase of OH. Nguyen and Dabdub (2002) calculated the detailed
71 isopleth between nitrate and NO_x emissions; they found that the reduction of NO_x
72 emissions resulted in a decrease of nitrate in the NO_x -limited regime, and an increase
73 of nitrate under extreme conditions in the VOC-limited regime. Despite that, the
74 single-site box model results could not distinguish the regional differences among
75 chemical regimes; the basic hypotheses in box models to predict nitrate production are
76 also unreasonable in the real atmosphere.

77 As an important precursor for both fine particles and ozone, the strict control of
78 NO_x emissions has started in China since the 12th Five-Year Plan (Zheng et al., 2018).
79 A confounding factor is that, for most cities in China, the production of O_3 is usually
80 limited by VOC_s (Xie et al., 2014; Dong et al., 2014; Liu et al., 2010). The control of
81 NO_x emissions has therefore resulted in an increase of surface O_3 concentrations in
82 recent years (Li et al., 2021a; Li et al., 2019a; Kalsoom et al., 2021), implying
83 complex impacts on nitrate formation. Li et al. (2021a) and Liu and Wang (2020)
84 examined the influencing factors on the surface O_3 trends in China from 2013 to 2017
85 using regional chemical models. They highlighted that the control of NO_x emissions
86 explained 11–35% of the increased O_3 due to the nonlinear NO_x - VOC_s - O_3 chemistry,
87 and that for most regions the magnitudes could be comparable to those resulting from
88 the meteorological influences and aerosol effects. Some simulations thought that the

89 NO_x emission increase in 2005–2012 resulted in an increase of nitrate by 3.4% yr⁻¹ in
90 eastern China (Geng et al., 2017; Wang et al., 2013), and the following NO_x emission
91 control resulted in a decrease of nitrate by 3–14% (Wang et al., 2014). Recent
92 evidence from field observations (Fu et al., 2020) and numerical simulations (Dong et
93 al., 2014), however, suggested that the NO_x emission reduction in China could result
94 in an increase of nitrate in winter through increased photochemical oxidants and
95 nocturnal N₂O₅ chemistry, but a decrease in other seasons. In the next 5–10 years,
96 SO₂ emissions might level off in China, while NO_x emissions will become stringently
97 controlled to ensure further air quality improvements (Zheng et al., 2018). Accurately
98 understanding the nonlinear aerosol and photochemistry feedbacks is crucial to
99 resolve the emerging nitrate pollution and to establish reasonable air pollution control
100 strategies in China.

101 To address this issue, we use comprehensive measurements and a regional
102 meteorology-chemistry model combined with hypothetical NO_x emission scenarios to
103 establish the nonlinear response relationships between particulate nitrate and NO_x
104 emission controls in the megalopolises of China. The model configurations, numerical
105 designs and observational data are presented in Sect. 2. Sect. 3 discusses the results.
106 Finally, a summary is presented in Sect. 4.

107 **2 Materials and Methods**

108 **2.1 Model setup and experimental designs**

109 This study uses the Weather Research and Forecasting-Chemistry (WRF-Chem)
110 model version 4.1 developed by Grell et al. (2002) to simulate the regional
111 meteorology and atmospheric chemistry. The mesoscale meteorology and air quality
112 simulations of WRF-Chem have been improved in terms of incorporating the satellite-
113 derived land surface parameters (Li et al., 2014; Li et al., 2017), and optimizing the

114 SIA formation pathways enhanced by mineral aerosols (Li et al., 2019b; Huang et al.,
115 2014b).

116 The modeling domain covers two main megalopolises of China and its adjacent
117 areas—the Beijing-Tianjin-Hebei (BTH) region and the Yangtze River Delta (YRD)
118 region (Fig. 1). The modeling framework is configured with 81×86 grid cells at 25 km
119 horizontal resolution. The model is run with an 84-hour model cycle, with the first 12
120 hours discarded as spin-up time and model outputs of each model cycle to provide
121 chemical initial conditions for the subsequent overlapping 84-hour simulation. The 6-
122 hour, 1°×1° National Centers for Environmental Prediction Final (NCEP/FNL)
123 analysis fields are regularly input for the model initial and lateral boundary
124 meteorological conditions.

125 The model physical configurations include the YSU boundary layer scheme
126 (Noh et al., 2003), the RRTMG radiation scheme (Iacono et al., 2008), the Noah land
127 surface scheme (Ek et al., 2003) and the Lin microphysics scheme (Lin et al., 1983).
128 We have updated the land cover type and vegetation data in WRF mesoscale model
129 with the latest land surface parameters derived from Moderate Resolution Imaging
130 Spectroradiometer (Li et al., 2014; Li et al., 2017).

131 The atmospheric chemistry is simulated using the Carbon Bond Mechanism
132 version Z (CBMZ) (Zaveri and Peters, 1999) gas-phase chemistry module coupled
133 with a four-bin sectional Model for Simulating Aerosol Interactions and Chemistry
134 (MOSAIC) (Zaveri et al., 2008). The aqueous-phase chemistry is based on the
135 Carnegie Mellon University (CMU) scheme including 50 species and more than 100
136 reactions (Fahey and Pandis, 2001). Formation of SIA in the default WRF-Chem
137 model accounts for the gas-phases oxidation of SO₂ and NO₂, and aqueous-phase
138 oxidation of SO₂ by hydrogen peroxide (H₂O₂) and O₃ in cloud. We have optimized

139 the SIA formation pathways by including the aqueous SO₂ oxidation catalyzed by
140 mineral ions and heterogeneous uptakes of SO₂, NO₂, NO₃, N₂O₅ and HNO₃ on
141 mineral aerosols in the MOSAIC aerosol module (Li et al., 2019b; Huang et al.,
142 2014b).

143 Anthropogenic emissions are adopted from the 2016 Multi-resolution Emission
144 Inventory for China (MEIC) and the 2010 MIX-Asia emission inventory for regions
145 outside of mainland China developed by Tsinghua University (<http://meicmodel.org>).
146 Biogenic emissions are calculated online using the Model of Emissions of Gases and
147 Aerosols from Nature (Guenther et al., 2006).

148 A series of WRF-Chem simulations is designed as summarized in Table 1. In the
149 baseline simulation (denoted as the B0 scenario), the anthropogenic emissions in
150 China remain unchanged at the usual levels in 2016. Simulation N0 is the same as B0,
151 but it only considers the gas-phase oxidation production of HNO₃ (NO₂+OH→HNO₃)
152 and its subsequent partitioning to the aerosol phase of nitrate in WRF-Chem. The B0
153 and N0 simulations are combined to distinguish the contributions of gas-phase
154 oxidation and heterogeneous pathways (i.e., uptakes of N₂O₅, NO₃ and NO₂) for the
155 formation of nitrate aerosols during the warm and cold seasons. A group of sensitivity
156 scenarios (C1~C8) are designed with the perturbed anthropogenic NO_x emissions in
157 China cut by 10%, 20%...and 80%, respectively. The differences between B0 and
158 C1~C8 simulations are calculated to illustrate the responses of particulate pollution in
159 China's megacities to the NO_x emission reduction scenarios. Another simulation (E1)
160 is designed with the anthropogenic emissions of NO_x in China set to the 2012 levels
161 to show the impacts of 2012–2016 NO_x control strategy on particulate pollution.
162 Additionally, in order to evaluate the effectiveness of multi-pollutants cooperative
163 controls, three series of simulations (C_{S-N}, C_{N-N} and C_{V-N}) are also supplemented with

164 the anthropogenic emissions of SO₂, NH₃ and VOC_s in China cut by 20%, 40%...and
165 80%, respectively. The differences between B0 and C_N/C_{S-N}/C_{N-N}/C_{V-N} simulations are
166 calculated to illustrate the responses of nitrate pollution in China's megacities to the
167 multi-pollutants cooperative controls.

168 For all simulation scenarios, two month-long periods during the Campaign on
169 Air Pollution and Urban Meteorology in Yangtze River Delta (CAPUM-YRD)—
170 August 15 to September 16 (Period I) and November 24 to December 26 (Period II) in
171 2016, are simulated to represent the warm and cold seasons, respectively (Shu et al.,
172 2019). The complete simulation consists of thirteen 84-hour model cycles with the
173 first 6 days as spin-up for chemistry and the remaining model outputs for analysis.

174 **2.2 Weather and air pollutants data**

175 Surface meteorological observations at 186 land-based automatic stations across
176 China (Fig. 1) are collected for model meteorological validation, including hourly
177 data of 2 m air temperature, 2 m relative humidity and 10 m wind speed. These data
178 are archived at the U. S. National Climatic Data Center (NCDC) (Smith et al., 2011).

179 Air pollutants data at the national air quality monitoring network and regional
180 supersites of China (Fig. 1) are used for model chemical validation. This nationwide
181 monitoring network contains 1597 sites covering 454 cities in mainland China, as
182 shown in Fig. 1. Six routine air pollutants including PM_{2.5}, particulate matter with
183 aerodynamic diameter less than 10 μm (PM₁₀), SO₂, NO₂, carbon monoxide (CO) and
184 O₃ are monitored and reported hourly by Chinese National Environmental Monitoring
185 Center (CNEMC) network (available at <http://websearch.mep.gov.cn/>).

186 Additionally, four comprehensive atmospheric environment supersites in YRD
187 including Dianshanhu (DSH; 31.1°N, 121.0°E), Pudong (PD; 31.2° N, 121.5°E),
188 Nanjing (NJ; 32.1°N, 118.8°E) and Hangzhou (HZ; 30.3°N, 120.2°E) measured the

189 mass concentrations of PM_{2.5}, water-soluble ions (sulfate, nitrate, ammonium, sodium,
190 chloride, potassium, calcium and magnesium), carbonaceous aerosols (elemental
191 carbon (EC) and organic carbon (OC)) and gaseous pollutants (SO₂, NO₂, CO and O₃)
192 during the CAPUM-YRD campaign. Details for the methods and data at the four
193 supersites are described in Shu et al. (2019).

194 **3 Results and discussions**

195 **3.1 Model weather and chemical validation**

196 Model evaluations indicate that the WRF-Chem model is able to simulate the
197 weather and atmospheric pollution characteristics in China. The simulated magnitudes
198 of surface temperature by WRF-Chem in general agree with actual observations, with
199 a correlation coefficient (*R*) of 0.89 and 0.94, and a normalized mean bias (NMB) of
200 -0.55% and -0.80% respectively in Period I and Period II (Table 2). Underestimation
201 of relative humidity (-5.65% in Period I and -6.56% in Period II) is common in the
202 WRF simulation and it might be attributed to the influence of the boundary layer
203 parameterization on the weather forecast (Bhati and Mohan, 2018; Gomez-Navarro et
204 al., 2015). Clear overestimation of wind speed (23.72% in Period I and 40.64% in
205 Period II) might be because of the unresolved topography in WRF (Jimenez et al.,
206 2013; Li et al., 2014).

207 The predicted concentrations of routine air pollutants also faithfully capture the
208 spatial and seasonal patterns of observed surface PM_{2.5}, SO₂, NO₂ and O₃ levels in
209 both seasons (Fig. 2). Both simulations and observations display high air pollutants
210 concentrations in the vicinity of North China Plain (NCP) and eastern China, but with
211 higher O₃ levels in the warm season and oppositely higher PM_{2.5} and other gaseous
212 pollutants concentrations in winter. The model statistical evaluations show a mean
213 bias (MB) of -3.66 , -1.14 , 4.70 and $18.32 \mu\text{g m}^{-3}$, and NMB of -9.92 , -6.46 , 16.47

214 and 7.72% for PM_{2.5}, SO₂, NO₂ and O₃ in Period I, and a relatively larger MB of
215 -27.31, -11.65, 1.27 and -39.01 $\mu\text{g m}^{-3}$, and NMB of -29.82, -28.11, 2.40 and
216 -31.05% in Period II, respectively (Table 3). The uncertainty in emissions data, the
217 absence of secondary organic aerosol in MOSAIC aerosol chemistry or the simulated
218 wind errors (Table 2) may be responsible for the larger atmospheric chemical biases
219 in winter, which has been extensively discussed in some studies (Zhao et al., 2016; Li
220 et al., 2021a).

221 As the most important components of PM_{2.5}, reasonable representation of SIA is
222 imperative to PM_{2.5} simulation. Evaluations with measurements of PM_{2.5} components
223 at the four supersites of eastern China show that the model performs reasonably in
224 simulating the seasonal variations and proportions of aerosol species in PM_{2.5}, but it is
225 biased low by 10–40% in simulating the magnitudes of SIA concentrations (Fig. 3).
226 The model underestimation is -1.8, -2.2 and -2.2 $\mu\text{g m}^{-3}$ for sulfate, nitrate and
227 ammonium, respectively, in Period I, and -2.6, -4.3 and -3.4 $\mu\text{g m}^{-3}$ in Period II. The
228 model also captures the large change of N/S ratio from the warm to cold seasons, that
229 increases from 0.4 in Period I to 1.6 in Period II. Our previous work (Li et al., 2019)
230 has confirmed that the consideration of the optimized aqueous and heterogeneous SIA
231 formation pathways in WRF-Chem significantly reduces the model biases by 41.4%
232 for sulfate and 44.6% for nitrate during the CAPUM-YRD campaign of 2016. Recent
233 studies highlighted that the remaining SIA simulation biases may be attributed to the
234 missing aqueous oxidation of SO₂ by NO₂ on alkaline aerosols under humid
235 conditions (Wang et al., 2016; Cheng et al., 2016).

236 **3.2 Air pollution and aerosol composition characteristics**

237 Chemical composition analyses of major gaseous and particulate air pollutants
238 suggest large seasonal variations of air pollution characteristics in China (Fig. 2).

239 Mainly emitted from combustion sources, atmospheric pollutants accumulate in the
240 densely industrialized and populated megalopolises of China, with a hotspot along
241 Beijing, Hebei, Shandong and their adjacent cities frequently exceeding China's
242 National Ambient Air Quality Standards. The average concentrations of surface PM_{2.5},
243 SO₂, NO₂ and daily-maximum O₃ in China's routine air quality monitoring network
244 are 33.8, 15.8, 26.5 and 223.2 μg m⁻³ for Period I, and 80.2, 34.7, 47.7 and 131.4 μg
245 m⁻³ for Period II. The surface PM_{2.5}, SO₂ and NO₂ concentrations show obvious
246 increases by 137.6%, 119.2% and 80.2% during winter compared to those of the
247 summer-autumn period (Period I). The maximum surface PM_{2.5} concentrations
248 recorded in the winter period was more than 600 μg m⁻³, which is the highest value
249 ever recorded in 2016 and leads to the "orange" air quality alert.

250 The further analyses of PM_{2.5} mass concentrations, major PM_{2.5} components and
251 gases at the four supersites in YRD are presented in Fig. 4–5. Organic matter (OM) is
252 obtained by multiplying the OC concentrations by a factor of 1.6, mainly accounting
253 for the hydrogen and oxygen masses in OM. The measured SIA concentrations
254 exhibit high levels, with average values of 18.8 μg m⁻³ for Period I and 37.1 μg m⁻³
255 for Period II. The three SIA components together account for 32.3–57.4% (48.6% on
256 average) and 27.7–70.9% (56.9% on average) of the total PM_{2.5} mass concentrations,
257 and become the primary components of PM_{2.5} in the two periods. The proportions of
258 sulfate, nitrate and ammonium in total PM_{2.5} range from 13.5–28.9%, 9.4–15.5% and
259 9.4–14.9% at the four supersites for Period I, and 9.2–20.3%, 11.5–32.1% and 7.0–
260 19.8% for Period II, respectively. The strikingly higher proportion of nitrate than that
261 of sulfate in PM_{2.5} during winter, with a N/S ratio of 1.6, is in accordance with recent
262 observations during other winter haze periods in China (Shao et al., 2018; Zhang et al.,
263 2018; Zhang et al., 2019). They emphasized that since the enactment of Clean Air

264 Action Plan in 2013, the PM_{2.5} components had changed clearly with decreasing
265 contributions from coal combustion.

266 The high proportions of sulfate and nitrate in PM_{2.5} could be related to the high
267 oxidation rates of SO₂ and NO₂. The observed average values of sulfur oxidation ratio
268 ($SOR = [SO_4^{2-}] / ([SO_4^{2-}] + [SO_2])$) and nitrogen oxidation ratio ($NOR = [NO_3^-] / ([NO_3^-]$
269 $+ [NO_2])$) are 0.41 and 0.13 in Period I, and 0.33 and 0.21 in Period II. In contrast, the
270 observed SOR is generally higher in summer-autumn than winter, opposite to that of
271 NOR, indicating the enhanced formation of nitrate in winter. Shu et al. (2019) also
272 noted similar seasonal distinctions for SOR and NOR in YRD. They attributed the
273 weakened conversion from NO₂ to nitrate in summer to the volatility and evaporative
274 loss of nitrate (Sun et al., 2012). The sharp increase of particles and moderate ambient
275 humidity in winter also benefit the heterogeneous formation of SIA, leading to high
276 NOR and SOR (Wang et al., 2012).

277 Figure 6 illustrates the contributions of gas-phase oxidation and heterogeneous
278 reactions for the nitrate production calculated from B0 and E0 simulations. It is shown
279 that on a daily basis the gas-phase oxidation production of HNO₃ and its subsequent
280 partitioning to the aerosol phase is the principal formation route for particulate nitrate,
281 with the average contributions of 60.2% for BTH and 91.7% for YRD in Period I and
282 75.1% for BTH and 85.9% for YRD in Period II. The heterogeneous hydrolyses of
283 N₂O₅ and other nitrogenous gases (calculated as the model differences between B0
284 and N0 simulations) contribute to the remaining nitrate, particularly in BTH with high
285 aerosol loading. These calculated results (60.2–91.7% for NO₂+OH oxidation and
286 8.3–39.8% for heterogeneous pathways) are in line with previous assessments in
287 China and globally. Alexander et al. (2009) reported that the global tropospheric
288 nitrate burden is dominated by NO₂+OH (76%), followed by N₂O₅ hydrolysis (18%);

289 but recent results suggested that N_2O_5 hydrolysis was as important as $\text{NO}_2 + \text{OH}$ (both
290 41 %) for global nitrate production (Alexander et al., 2020). In major Chinese cities, it
291 was estimated that the conversion of NO_x to nitrate was dominated by $\text{NO}_2 + \text{OH}$
292 oxidation in Shanghai, with a mean contribution of 55–77% in total and even higher
293 (84–92%) in summer (He et al., 2020). In NCP, the nitrate contribution of
294 heterogeneous pathways was about 30.8% (Liu et al., 2020) or even comparable to the
295 partitioning of HNO_3 (Wang et al., 2019; Wang et al., 2017a; Luo et al., 2021). The
296 nitrate formation from heterogeneous pathways is moderately underestimated in the
297 optimized WRF-Chem model of this study, possibly due to the uncertainties of
298 heterogeneous uptake coefficients and unclear reaction mechanisms applied in the
299 model (Li et al., 2019b; Xue et al., 2016; He et al., 2014).

300 **3.3 Nonlinear responses of nitrate to NO_x emissions and their policy implications**

301 **3.3.1 $\text{PM}_{2.5}$ - NO_x and O_3 - NO_x responses in the warm and cold seasons**

302 NO_x is key in atmospheric chemistry and serves as an important precursor for
303 both ozone and secondary aerosols. We conduct a series of simulations (C1~C8) with
304 perturbed NO_x emissions to assess the responses of $\text{PM}_{2.5}$ mass concentrations to NO_x
305 emissions in two megalopolises of China (Fig. 7). The WRF-Chem simulation results
306 show that the responses of surface $\text{PM}_{2.5}$ concentrations to NO_x emissions vary in
307 different seasons and display strong nonlinear behaviour in winter. To better quantify
308 their effectiveness, we define the NO_x emission control efficiency (β), which denotes
309 the percentage changes of surface $\text{PM}_{2.5}$ or its components concentrations in response
310 to the successive 10% cut of NO_x emissions.

311 In Period I (Aug–Sep), the $\text{PM}_{2.5}$ - NO_x responses are closer to a linear function,
312 reflecting a stronger sensitivity to the NO_x emission changes in the warm season. The
313 surface $\text{PM}_{2.5}$ concentrations decrease almost linearly as we gradually reduce NO_x

314 emissions in China, with the average β values of -2.2% in BTH and -2.9% in YRD.
315 However, the $\text{PM}_{2.5}$ - NO_x emission responses in Period II (Nov–Dec) display strong
316 nonlinearity and are analogous to a quadratic parabola distribution for both regions.
317 The NO_x emission reductions within the first 50% would even increase surface $\text{PM}_{2.5}$
318 concentrations by $+1.2\%$ averagely in BTH, and this β value increases to $+1.8\%$ in
319 YRD with the first 40% reductions of NO_x emissions. Subsequently, the $\text{PM}_{2.5}$
320 responses shift towards a similar linear pattern, with an average β value of -2.5% in
321 BTH and -4.0% in YRD.

322 The distinct forms of $\text{PM}_{2.5}$ - NO_x emission responses for the warm and cold
323 seasons are determined by the seasonal ozone chemical sensitivity regimes. The
324 photochemical indicator of $\Delta[\text{O}_3]_{\text{NO}_x}/\Delta[\text{O}_3]_{\text{VOC}_s}$ with a critical value of 1.0 is used to
325 investigate the season-varying ozone sensitivity in China, which is calculated as the
326 ratio of ozone concentration changes under 20% NO_x emission reduction to that under
327 20% VOC_s emission reduction (Fig. S1). The results indicate a strong VOC-limited
328 ozone chemistry across China during winter, while either VOC-limited regime over a
329 large portion of NCP and eastern China or NO_x -limited regime in northern and
330 western China during summer-autumn, as also indicated from previous studies (Xie et
331 al., 2014; Dong et al., 2014; Liu et al., 2010). We find larger O_3 and OH productions
332 under the NO_x emission reduction conditions in both seasons (Fig. 8–9), particularly
333 in Period II (Nov–Dec) with an average increase rate of $+14.7\%$ and $+18.5\%$ in BTH
334 and $+25.2\%$ and $+23.1\%$ in YRD per 10% cut of NO_x emissions. The SIA formation
335 chemistry is highly limited by atmospheric oxidants produced from the NO_x - VOC_s - O_3
336 photochemical cycles. The nonlinear O_3 - NO_x responses indicate a rather complicated
337 aerosol and photochemistry feedback in megacities.

338 3.3.2 Nonlinear responses of particulate nitrate to NO_x emissions

339 The SIA formation is basically driven by the atmospheric oxidants levels, and a
340 reduction of NO_x emissions may have counter-intuitive effects on SIA components by
341 controlling the atmospheric oxidants levels. The calculated SIA components for each
342 emission scenario in both months show that the surface nitrate aerosols can be
343 substantially decreased/increased with reducing NO_x emissions, but the sulfate and
344 ammonium concentrations have moderately smaller changes (Fig. 8–10).

345 Response of sulfate to the NO_x emissions is more predictable and determined by
346 the changes of atmospheric oxidants levels since that the conversion of SO₂ to sulfate
347 is partly driven by OH in the gas-phase and by dissolved H₂O₂ or O₃ in the presence
348 of fog or cloud. In Period I (Aug–Sep), the sulfate-NO_x response follows a gradual
349 quadratic parabola distribution as that of O₃-NO_x and OH-NO_x response curves (Fig.
350 8 and Fig. 10), with a fitted function in Eq. 1. The β values for surface sulfate change
351 by -0.7%~+1.2% in BTH and -1.5%~+0.2% in YRD under each NO_x emission
352 reduction scenarios.

$$353 \quad [\text{SO}_4^{2-}] = -2.4\Delta E_{\text{NO}_x}^2 - 1.7\Delta E_{\text{NO}_x} + 6.1 \text{ in BTH} \quad (R^2=0.93) \quad (\text{Eq. 1})$$

$$354 \quad [\text{SO}_4^{2-}] = -2.3\Delta E_{\text{NO}_x}^2 - 0.9\Delta E_{\text{NO}_x} + 6.8 \text{ in YRD} \quad (R^2=0.99)$$

355 where [SO₄²⁻] is the surface mean concentration of sulfate (μg m⁻³); ΔE_{NO_x} is the
356 percentage change of NO_x emissions (%).

357 As expected, the production of nitrate reflects a strong sensitivity to NO_x and it
358 decreases linearly with the NO_x emission control, with an average β value of -10.2%
359 in BTH and -11.5% in YRD, which further leads to a decrease of ammonium
360 concentrations by -3.3% in BTH and -4.3% in YRD (Fig. 8 and Fig. 10). The
361 formation of nitrate mainly involves the NO₂+OH→HNO₃ gas-phase oxidation and
362 the heterogeneous hydrolysis of N₂O₅ and other nitrogenous gases. The strong

363 sensibility of particulate nitrate in response to the NO_x emission decreases can be
 364 explained by the synchronously suppressive production of its intermediate products
 365 HNO₃ and N₂O₅. For example, when the NO_x emission is cut by 20%, the surface
 366 NO₂ concentration in BTH drops by 20.0% but the surface O₃ and OH concentrations
 367 increase slightly by 2.6% and 5.3% due to the reduction of NO+O₃ titration reaction
 368 and the greater VOC availability in the warm season, leading to substantial reductions
 369 in surface HNO₃ (-16.7%) and N₂O₅ (-8.9%) concentrations.

370
$$[\text{NO}_3^-] = -34.5\Delta E_{\text{NO}_x}^2 - 23.8\Delta E_{\text{NO}_x} + 13.2 \text{ in BTH} \quad (R^2=0.84) \quad (\text{Eq. 2})$$

371
$$[\text{NO}_3^-] = -36.5\Delta E_{\text{NO}_x}^2 - 19.6\Delta E_{\text{NO}_x} + 12.0 \text{ in YRD} \quad (R^2=0.99)$$

372
$$[\text{NH}_4^+] = -9.1\Delta E_{\text{NO}_x}^2 - 6.9\Delta E_{\text{NO}_x} + 6.2 \text{ in BTH} \quad (R^2=0.78) \quad (\text{Eq. 3})$$

373
$$[\text{NH}_4^+] = -10.5\Delta E_{\text{NO}_x}^2 - 6.2\Delta E_{\text{NO}_x} + 5.3 \text{ in YRD} \quad (R^2=0.98)$$

374 where [NO₃⁻] and [NH₄⁺] are the surface mean concentrations (μg m⁻³) of nitrate
 375 and ammonium, respectively.

376 In Period II (Nov–Dec), we find opposite results with quadratic parabola
 377 distributions for nitrate-NO_x response (Eq. 2) and ammonium-NO_x response (Eq. 3),
 378 but linearly increasing sulfate concentrations (average β values of +2.0% in BTH and
 379 +2.6% in YRD; Fig. 9 and Fig. 10), leading to small PM_{2.5} changes in winter. Such
 380 nonlinear nitrate-NO_x responses can be explained by the substantially increased
 381 oxidants as we gradually reduce NO_x emissions in each scenario. It is noted that in
 382 winter the nitrate-NO_x response highly depends on the production of N₂O₅, which is
 383 produced from the $\text{NO}_2 \xrightarrow{\text{O}_3} \text{NO}_3 \xrightarrow{\text{NO}_2} \text{N}_2\text{O}_5$ chemical reactions and is a crucial intermediate
 384 product for nitrate formation. Under the low NO_x emission reduction conditions, the
 385 production of N₂O₅ is more sensitive to the atmospheric oxidants concentrations. The
 386 significant increases of surface O₃ in each NO_x emission scenario in the VOC-poor

387 environment (Fig. 9(b, d)) lead to an enhancement of N_2O_5 levels from 10% to more
388 than 100%. In spite of the HNO_3 concentration remaining nearly unchanged or
389 decreasing slightly by less than 5% in response to NO_x control, nitrate is found to
390 increase (average β values of +4.1% in BTH and +5.1% in YRD) with higher N_2O_5
391 produced from the increased ozone introduced by attenuated titration. An inflexion
392 point appears at the 40–50% NO_x emission reduction scenario, and a further reduction
393 in NO_x emissions is predicted to cause –10.5% and –5.3% reductions of surface
394 particulate nitrate and ammonium for BTH, and –7.7% and –7.4% for YRD.

395 These results reveal that the increase in atmospheric oxidants in response to NO_x
396 emission control can offset the decreasing precursors concentrations and further
397 enhance the formation of secondary nitrate, as recently found during the COVID-19
398 pandemic (Huang et al., 2020; Li et al., 2021b).

399 **3.3.3 Impacts of 2012–2016 NO_x control strategy on particulate pollution**

400 During the 12th Five-Year Plan period (2011–2015), a series of end-of-pipe
401 pollutant controls (e.g., Selective Catalytic Reduction techniques) were carried out for
402 power, industry and transportation sectors. These measures effectively controlled the
403 national NO_x emissions by 22.8% from 2012 to 2016 (MEIC v1.3) in China. To
404 quantify the effects of recent NO_x control measures on the levels of photochemical
405 oxidants and particulate nitrate, we conduct an additional simulation with NO_x
406 emissions set to the levels of 2012 in E1.

407 The model simulations (Fig. 11) suggest that reducing China's NO_x emissions
408 alone from 2012 to 2016 leads to an average –24.9%~–8.6% decrease of NO_x
409 concentrations in the surface layer. As previously pointed out, the 2012–2016 NO_x
410 emission control measures lead to increased O_3 and OH levels in winter, which offset
411 the effectiveness of NO_x emission reduction in alleviating winter nitrate. No obvious

412 declines in the winter nitrate levels are observed and even increases in some areas
413 (+8.8% in BTH and 14.4% in YRD; Fig. S2–S3). As shown, the largest PM_{2.5}
414 responses shift towards the southern Hebei and central China provinces, where the
415 wintertime PM_{2.5} concentrations are particularly high in this region. The substantial
416 emission changes from 2012 to 2016 lower the PM_{2.5} air pollution by up to –1.8% in
417 BTH and –3.5% in YRD for Period I and oppositely increase the surface PM_{2.5} by
418 2.4% in BTH and 4.7% in YRD for Period II. The past NO_x emission control strategy
419 leads to increased atmospheric oxidants levels and deteriorated particulate pollution in
420 winter due to the nonlinear photochemistry and aerosol chemical feedbacks, without
421 regard to the other emission control measures. This conclusion is also supported by
422 evidence from the recent field observations (Fu et al., 2020).

423 **3.3.4 Responses of particulate nitrate to multi-pollutants cooperative controls**

424 In order to evaluate the effectiveness of multi-pollutants cooperative controls in
425 China, three series of additional simulations (C_{S-N} , C_{N-N} and C_{V-N}) are also designed to
426 show the responses of nitrate and PM_{2.5} pollution to the emission controls of NO_x,
427 SO₂, NH₃ and VOC_s, respectively. The results (Fig. 12) show that atmospheric NH₃
428 and VOC_s are effective in controlling the particulate nitrate pollution for both seasons,
429 whereas decreasing the SO₂ and NO_x emissions may have counter-intuitive effects on
430 the concentration levels of nitrate aerosols.

431 Atmospheric NH₃ acts as a critical neutralizing species for SIA production and
432 efficient haze mitigation (Liu et al., 2019). According to the WRF-Chem simulation,
433 reduction of NH₃ emissions may be effective in reducing the nitrate component, with
434 an average β value of –10.0% in BTH and –10.3% in YRD for Period I, and –8.3% in
435 BTH and –11.5% in YRD for Period II, primarily by suppressing the ammonium
436 nitrate formation. Quantitatively, a 10% reduction in NH₃ emissions can alleviate the

437 PM_{2.5} pollution by -2.7% during summer-autumn and -3.2% during winter in the two
438 Chinese megacities. Atmospheric chemistry modeling by Wen et al. (2021) also
439 indicated that controlling NH₃ emissions in Beijing would significantly reduce the
440 population-weighted PM_{2.5} concentrations by 6.2–21% with 60–100% NH₃ reductions
441 in January, implying the need to consider NH₃ emission controls when designing the
442 PM_{2.5} pollution mitigation strategies.

443 VOC_s, which is not a direct precursor for SIA, is effective in SIA controls due to
444 their influences on the atmospheric oxidation cycles (Tsimpidi et al., 2008; Womack
445 et al., 2019; Nguyen and Dabdub, 2002). Our results suggest that decreasing VOC_s
446 emissions per 10% would suppress the oxidation formation of nitrate and decrease the
447 nitrate concentrations by -2.5% in BTH and -1.7% in YRD for Period I, and -5.0%
448 in BTH and -6.3% in YRD for Period II. The reduction of VOC_s emissions would
449 result in a decrease of PM_{2.5} by -0.7% during summer-autumn and -1.8% during
450 winter in the two megacities. Tsimpidi et al. (2008) also showed that the reduction of
451 VOC_s emissions caused a marginal increase of PM_{2.5} during summer in eastern United
452 States, whereas it resulted in a decrease of atmospheric oxidant levels and 5–20%
453 reduction of both inorganic and organic PM_{2.5} components during winter. Larger and
454 synchronized NO_x and VOC_s emissions controls are required to overcome the adverse
455 effects of nonlinear photochemistry and aerosol chemical feedbacks.

456 The SO₂ emission reduction, although effective in reducing sulfate and PM_{2.5}, is
457 not successful in regulating the nitrate pollution due to the chemical competition in
458 nitrate and sulfate formations (Geng et al., 2017; Wang et al., 2013). Changes in
459 nitrate concentration are linearly associated with the SO₂ emission reductions, with
460 the average β values of 2.9% during summer-autumn and 1.3% during winter.
461 Decreasing SO₂ emissions is less effective (a β value of -0.7%) in mitigating the

462 wintertime haze pollution because that the benefit of SO₂ reduction is partly offset by
463 the significant increase of nitrate, demonstrating the critical role of multi-pollutants
464 cooperative controls. Lei et al. (2013) evaluated the impacts of SO₂ control strategies
465 on nitrate and sulfate production in USA and also found that the competition for bases
466 in nitrate and sulfate formation significantly affects the nitrate concentrations.

467 Our results emphasize that future nitrate and PM_{2.5} pollution mitigation strategies
468 should focus on reducing the chemical precursors and key atmospheric oxidants
469 involved in the production of secondary aerosols. The recent “Three-year Action Plan
470 Fighting for a Blue Sky” calls for stringent emissions controls of NO_x, SO₂, VOC_s and
471 NH₃ but without specific reduction targets. Such emission changes would emphasize
472 the need to jointly consider multi-pollutants emissions controls for mitigating haze air
473 pollution.

474 **4 Conclusions**

475 Recent air pollution actions have significantly lowered the PM_{2.5} levels in China
476 via controlling emissions of SO₂ and NO_x, but raised a new question of how effective
477 the NO_x emission controls can be on the mitigation of emerging nitrate and ozone air
478 pollution. We use comprehensive measurements and a regional meteorology-
479 chemistry model with optimized mechanisms to establish the nonlinear responses
480 between particulate nitrate and NO_x emission controls in the megalopolises of China.

481 Nitrate is an essential component of PM_{2.5} in eastern China, accounting for 9.4–
482 15.5% and 11.5–32.1% of the total PM_{2.5} mass for the warm and cold seasons,
483 respectively. We find that the efficiency of PM_{2.5} reduction is highly sensitive to NO_x
484 emissions and it varies in different seasons depending on the ozone chemical regimes.
485 The reduction of NO_x emissions results in almost linearly lower PM_{2.5} by –2.2% in
486 BTH and –2.9% in YRD per 10% cut of NO_x emissions during summer-autumn,

487 whereas it increases the atmospheric oxidants levels and leads to a rather complicated
488 response of the PM components in winter. Nitrate is found to increase (average β
489 values of +4.1% in BTH and +5.1% in YRD) in winter with higher N_2O_5 intermediate
490 produced from the increased ozone introduced by attenuated titration, despite the
491 nearly unchanged or slightly decreased HNO_3 concentrations in response to NO_x
492 control. An inflexion point appears at 40–50% NO_x emission reduction, and a further
493 reduction of NO_x emissions is predicted to cause –10.5% reductions of particulate
494 nitrate for BTH and –7.7% for YRD. In addition, the 2012–2016 NO_x emission
495 control strategy leads to –24.9%––8.6% decreases of surface NO_x concentrations, and
496 no changes or even increases of wintertime nitrate in BTH (+8.8%) and YRD (14.4%).
497 Our results also emphasize that atmospheric NH_3 and VOC_s are effective in
498 controlling the particulate nitrate pollution, whereas decreasing the SO_2 and NO_x
499 emissions may have counter-intuitive effects on nitrate aerosols. These results provide
500 insights for developing mitigation strategies for the ubiquitous nitrate aerosols in
501 winter haze of China.

502 **Author contribution**

503 Mengmeng Li developed the model code, designed the numerical experiments,
504 and wrote the original draft. Zihan Zhang carried out the numerical experiments.
505 Quan Yao provided and analyzed some of the data. Min Xie, Shu Li and Bingliang
506 Zhuang validated and analyzed the model results. Tijian Wang and Yong Han
507 reviewed and revised the manuscript.

508 **Competing interests**

509 The authors declare that they have no conflict of interest.

510 **Acknowledgement**

511 This study is funded by the National Natural Science Foundation of China

512 (41975153, 42077192 and 41775026), the National Key Basic Research Development
513 Program of China (2019YFC0214603, 2020YFA0607802), and the Emory
514 University-Nanjing University Collaborative Research Grant.

515 **Data availability statement**

516 The WRF-Chem model version 4.1 is available at
517 <http://www2.mmm.ucar.edu/wrf/users/downloads.html>. The NCEP FNL data are
518 accessible at the National Center for Atmospheric Research (NCAR) Research Data
519 Archive (RDA; <http://rda.ucar.edu/datasets/ds083.2/>). The MEIC anthropogenic
520 emission inventories are available at www.meicmodel.org, and for more information,
521 please contact Q. Zhang (qiangzhang@tsinghua.edu.cn). The surface weather data are
522 accessible at the Integrated Surface Database ([https://www.ncdc.noaa.gov/isd/data-](https://www.ncdc.noaa.gov/isd/data-access)
523 [access](https://www.ncdc.noaa.gov/isd/data-access)). The surface air pollutants and aerosol species data are provided by Chinese
524 National Environmental Monitoring Center (<http://www.cnemc.cn/en/>) and archived
525 at <https://doi.org/10.6084/m9.figshare.12818807.v1>.

526 **References**

527 Alexander, B., Hastings, M. G., Allman, D. J., Dachs, J., Thornton, J. A., and
528 Kunasek, S. A.: Quantifying atmospheric nitrate formation pathways based on a
529 global model of the oxygen isotopic composition (δ O-17) of atmospheric
530 nitrate, *Atmos Chem Phys*, 9, 5043-5056, 2009.

531 Alexander, B., Sherwen, T., Holmes, C. D., Fisher, J. A., Chen, Q. J., Evans, M. J.,
532 and Kasibhatla, P.: Global inorganic nitrate production mechanisms: comparison
533 of a global model with nitrate isotope observations, *Atmos Chem Phys*, 20,
534 3859-3877, 2020.

535 Bhati, S. and Mohan, M.: WRF-urban canopy model evaluation for the assessment of
536 heat island and thermal comfort over an urban airshed in India under varying
537 land use/land cover conditions, *Geosci Lett*, 5, doi: 10.1186/s40562-018-0126-7,
538 2018.

539 Cheng, Y. F., Zheng, G. J., Wei, C., Mu, Q., Zheng, B., Wang, Z. B., Gao, M., Zhang,
540 Q., He, K. B., Carmichael, G., Poschl, U., and Su, H.: Reactive nitrogen
541 chemistry in aerosol water as a source of sulfate during haze events in China, *Sci*
542 *Adv*, 2, e1601530, doi: 10.1126/sciadv.1601530, 2016.

543 Dong, X. Y., Li, J., Fu, J. S., Gao, Y., Huang, K., and Zhuang, G. S.: Inorganic
544 aerosols responses to emission changes in Yangtze River Delta, China, *Sci Total*
545 *Environ*, 481, 522-532, 2014.

546 Ek, M. B., Mitchell, K. E., Lin, Y., Rogers, E., Grunmann, P., Koren, V., Gayno, G.,
547 and Tarpley, J. D.: Implementation of Noah land surface model advances in the
548 National Centers for Environmental Prediction operational mesoscale Eta model,
549 *J Geophys Res-Atmos*, 108, 8851, doi: 10.1029/2002jd003296, 2003.

550 Fahey, K. M. and Pandis, S. N.: Optimizing model performance: variable size
551 resolution in cloud chemistry modeling, *Atmos Environ*, 35, 4471-4478, 2001.

552 Fu, X., Wang, T., Gao, J., Wang, P., Liu, Y. M., Wang, S. X., Zhao, B., and Xue, L.
553 K.: Persistent Heavy Winter Nitrate Pollution Driven by Increased
554 Photochemical Oxidants in Northern China, *Environ Sci Technol*, 54, 3881-3889,
555 2020.

556 Geng, G. N., Zhang, Q., Tong, D., Li, M., Zheng, Y. X., Wang, S. W., and He, K. B.:
557 Chemical composition of ambient PM_{2.5} over China and relationship to precursor
558 emissions during 2005-2012, *Atmos Chem Phys*, 17, 9187-9203, 2017.

559 Gomez-Navarro, J. J., Raible, C. C., and Dierer, S.: Sensitivity of the WRF model to
560 PBL parametrisations and nesting techniques: evaluation of wind storms over
561 complex terrain, *Geosci Model Dev*, 8, 3349-3363, 2015.

562 Grell, G. A., McKeen, S., Michalakes, J., Bao, J. W., Trainer, M., and Hsie, E. Y.:
563 Real-time simultaneous prediction of air pollution and weather during the
564 Houston 2000 field experiment, *Fourth Conference on Atmospheric Chemistry:*
565 *Urban, Regional And Global Scale Impacts Of Air Pollutants*, 224-227, 2002.

566 Guenther, A., Karl, T., Harley, P., Wiedinmyer, C., Palmer, P. I., and Geron, C.:
567 Estimates of global terrestrial isoprene emissions using MEGAN (Model of
568 Emissions of Gases and Aerosols from Nature), *Atmos Chem Phys*, 6, 3181-
569 3210, 2006.

570 He, H., Wang, Y. S., Ma, Q. X., Ma, J. Z., Chu, B. W., Ji, D. S., Tang, G. Q., Liu, C.,
571 Zhang, H. X., and Hao, J. M.: Mineral dust and NO_x promote the conversion of
572 SO₂ to sulfate in heavy pollution days, *Scientific Reports*, 4, 4172, doi:
573 10.1038/Srep04172, 2014.

574 He, P. Z., Xie, Z. Q., Yu, X. W., Wang, L. Q., Kang, H., and Yue, F. G.: The
575 observation of isotopic compositions of atmospheric nitrate in Shanghai China
576 and its implication for reactive nitrogen chemistry, *Sci Total Environ*, 714,
577 136727, doi: 10.1016/j.scitotenv.2020.136727, 2020.

578 He, P. Z., Xie, Z. Q., Chi, X. Y., Yu, X. W., Fan, S. D., Kang, H., Liu, C., and Zhan,
579 H. C.: Atmospheric Delta O-17(NO₃⁻) reveals nocturnal chemistry dominates
580 nitrate production in Beijing haze, *Atmos Chem Phys*, 18, 14465-14476, 2018.

581 Huang, R. J., Zhang, Y. L., Bozzetti, C., Ho, K. F., Cao, J. J., Han, Y. M.,
582 Daellenbach, K. R., Slowik, J. G., Platt, S. M., Canonaco, F., Zotter, P., Wolf, R.,
583 Pieber, S. M., Bruns, E. A., Crippa, M., Ciarelli, G., Piazzalunga, A.,
584 Schwikowski, M., Abbaszade, G., Schnelle-Kreis, J., Zimmermann, R., An, Z. S.,
585 Szidat, S., Baltensperger, U., El Haddad, I., and Prevot, A. S. H.: High secondary
586 aerosol contribution to particulate pollution during haze events in China, *Nature*,
587 514, 218-2222014a.

588 Huang, X., Song, Y., Zhao, C., Li, M. M., Zhu, T., Zhang, Q., and Zhang, X. Y.:
589 Pathways of sulfate enhancement by natural and anthropogenic mineral aerosols
590 in China, *J Geophys Res-Atmos*, 119, 14165-14179, 2014b.

591 Huang, X., Ding, A., Gao, J., Zheng, B., Zhou, D., Qi, X., Tang, R., Wang, J., Ren, C.,
592 Nie, W., Chi, X., Xu, Z., Chen, L., Li, Y., Che, F., Pang, N., Wang, H., Tong, D.,
593 Qin, W., Cheng, W., Liu, W., Fu, Q., Liu, B., Chai, F., Davis, S., Zhang, Q., and
594 He, K.: Enhanced secondary pollution offset reduction of primary emissions
595 during COVID-19 lockdown in China, *Natl Sci Rev*, 1-9, 2020.

596 Iacono, M. J., Delamere, J. S., Mlawer, E. J., Shephard, M. W., Clough, S. A., and
597 Collins, W. D.: Radiative forcing by long-lived greenhouse gases: Calculations
598 with the AER radiative transfer models, *J Geophys Res-Atmos*, 113, D13103,
599 doi: 10.1029/2008jd009944, 2008.

600 Jimenez, P. A., Dudhia, J., Gonzalez-Rouco, J. F., Montavez, J. P., Garcia-
601 Bustamante, E., Navarro, J., de Arellano, J. V. G., and Munoz-Roldan, A.: An
602 evaluation of WRF's ability to reproduce the surface wind over complex terrain
603 based on typical circulation patterns, *J Geophys Res-Atmos*, 118, 7651-7669,
604 2013.

605 Kalsoom, U., Wang, T. J., Ma, C. Q., Shu, L., Huang, C. W., and Gao, L. B.:
606 Quadrennial variability and trends of surface ozone across China during 2015-
607 2018: A regional approach, *Atmos Environ*, 245, 117989, doi:
608 10.1016/j.atmosenv.2020.117989, 2021.

609 Lei, H., Wuebbles, D. J.: Chemical competition in nitrate and sulfate formations and
610 its effect on air quality, *Atmos Environ*, 80, 472-477, 2013.

611 Li, K., Jacob, D. J., Liao, H., Shen, L., Zhang, Q., and Bates, K. H.: Anthropogenic
612 drivers of 2013-2017 trends in summer surface ozone in China, *P Natl Acad Sci*
613 *USA*, 116, 422-427, 2019a.

614 Li, M. M., Song, Y., Huang, X., Li, J. F., Mao, Y., Zhu, T., Cai, X. H., and Liu, B.:
615 Improving mesoscale modeling using satellite-derived land surface parameters in
616 the Pearl River Delta region, China, *J Geophys Res-Atmos*, 119, 6325-6346,
617 2014.

618 Li, M. M., Wang, T. J., Shu, L., Qu, Y. W., Xie, M., Liu, J. N., Wu, H., and Kalsoom,
619 U.: Rising surface ozone in China from 2013 to 2017: A response to the recent
620 atmospheric warming or pollutant controls?, *Atmos Environ*, 246, 118130, doi:
621 10.1016/j.atmosenv.2020.118130, 2021a.

622 Li, M. M., Wang, T. J., Xie, M., Zhuang, B. L., Li, S., Han, Y., Song, Y., and Cheng,
623 N. L.: Improved meteorology and ozone air quality simulations using MODIS
624 land surface parameters in the Yangtze River Delta urban cluster, China, *J*
625 *Geophys Res-Atmos*, 122, 3116-3140, 2017.

626 Li, M. M., Wang, T. J., Xie, M., Li, S., Zhuang, B. L., Huang, X., Chen, P. L., Zhao,
627 M., and Liu, J. E.: Formation and Evolution Mechanisms for Two Extreme Haze
628 Episodes in the Yangtze River Delta Region of China During Winter 2016, *J*
629 *Geophys Res-Atmos*, 124, 3607-3623, 2019b.

630 Li, M. M., Wang, T. J., Xie, M., Li, S., Zhuang, B. L., Fu, Q. Y., Zhao, M., Wu, H.,
631 Liu, J., Saikawa, E., and Liao, K.: Drivers for the poor air quality conditions in
632 North China Plain during the COVID-19 outbreak, *Atmos Environ*, 246, 118103,
633 doi: 10.1016/j.atmosenv.2020.118103, 2021b.

634 Lin, Y. L., Farley, R. D., and Orville, H. D.: Bulk Parameterization of the Snow Field
635 in a Cloud Model, *J Clim Appl Meteorol*, 22, 1065–1092, 1983.

636 Liu, L., Bei, N. F., Hu, B., Wu, J. R., Liu, S. X., Li, X., Wang, R. N., Liu, Z. R., Shen,
637 Z. X., and Li, G. H.: Wintertime nitrate formation pathways in the north China
638 plain: Importance of N₂O₅ heterogeneous hydrolysis, *Environ Pollut*, 266,
639 115287, doi: 10.1016/j.envpol.2020.115287, 2020.

640 Liu, M. X., Huang, X., Song, Y., Tang, J., Cao, J. J., Zhang, X. Y., Zhang, Q., Wang,
641 S. X., Xu, T. T., Kang, L., Cai, X. H., Zhang, H. S., Yang, F. M., Wang, H. B.,
642 Yu, J. Z., Lau, A. K. H., He, L. Y., Huang, X. F., Duan, L., Ding, A. J., Xue, L.
643 K., Gao, J., Liu, B., and Zhu, T.: Ammonia emission control in China would
644 mitigate haze pollution and nitrogen deposition, but worsen acid rain, *P Natl*
645 *Acad Sci USA*, 116, 7760-7765, 2019.

646 Liu, X. H., Zhang, Y., Xing, J., Zhang, Q. A., Wang, K., Streets, D. G., Jang, C.,
647 Wang, W. X., and Hao, J. M.: Understanding of regional air pollution over China
648 using CMAQ, part II. Process analysis and sensitivity of ozone and particulate
649 matter to precursor emissions, *Atmos Environ*, 44, 3719-3727, 2010.

650 Liu, Y. M. and Wang, T.: Worsening urban ozone pollution in China from 2013 to
651 2017-Part 2: The effects of emission changes and implications for multi-pollutant
652 control, *Atmos Chem Phys*, 20, 6323-6337, 2020.

653 Luo, L., Zhu, R. G., Song, C. B., Peng, J. F., Guo, W., Liu, Y. H., Zheng, N. J., Xiao,
654 H. W., and Xiao, H. Y.: Changes in nitrate accumulation mechanisms as PM_{2.5}
655 levels increase on the North China Plain: A perspective from the dual isotopic
656 compositions of nitrate, *Chemosphere*, 263, 127915, doi:
657 10.1016/j.chemosphere.2020.127915, 2021.

658 Meng, Z., Dabdub, D., and Seinfeld, J. H.: Chemical coupling between atmospheric
659 ozone and particulate matter, *Science*, 277, 116-119, 1997.

660 Nguyen, K. and Dabdub, D.: NO_x and VOC control and its effects on the formation
661 of aerosols, *Aerosol Sci Tech*, 36, 560-572, 2002.

662 Noh, Y., Cheon, W. G., Hong, S. Y., and Raasch, S.: Improvement of the K-profile
663 model for the planetary boundary layer based on large eddy simulation data,
664 *Bound-Lay Meteorol*, 107, 401–427, 2003.

665 Pathak, R. K., Wang, T., and Wu, W. S.: Nighttime enhancement of PM_{2.5} nitrate in
666 ammonia-poor atmospheric conditions in Beijing and Shanghai: Plausible
667 contributions of heterogeneous hydrolysis of N₂O₅ and HNO₃ partitioning,
668 *Atmos Environ*, 45, 1183-1191, 2011.

669 Pun, B. K. and Seigneur, C.: Sensitivity of particulate matter nitrate formation to
670 precursor emissions in the California San Joaquin Valley, *Environ Sci Technol*,
671 35, 2979-2987, 2001.

672 Seinfeld, J. H. and Pandis, S. N.: *Atmospheric chemistry and physics: from air
673 pollution to climate change*. 2nd Edition, John Wiley and Sons, Hoboken, NJ,
674 2006.

675 Shao, P. Y., Tian, H. Z., Sun, Y. J., Liu, H. J., Wu, B. B., Liu, S. H., Liu, X. Y., Wu,
676 Y. M., Liang, W. Z., Wang, Y., Gao, J. J., Xue, Y. F., Bai, X. X., Liu, W., Lin, S.
677 M., and Hu, G. Z.: Characterizing remarkable changes of severe haze events and
678 chemical compositions in multi-size airborne particles (PM₁, PM_{2.5} and PM₁₀)
679 from January 2013 to 2016-2017 winter in Beijing, China, *Atmos Environ*, 189,
680 133-144, 2018.

681 Shu, L., Wang, T. J., Xie, M., Li, M. M., Zhao, M., Zhang, M., and Zhao, X. Y.:
682 Episode study of fine particle and ozone during the CAPUM-YRD over Yangtze
683 River Delta of China: Characteristics and source attribution, *Atmos Environ*, 203,
684 87-101, 2019.

685 Silver, B., Reddington, C. L., Arnold, S. R., and Spracklen, D. V.: Substantial
686 changes in air pollution across China during 2015-2017, *Environ Res Lett*, 14,
687 114012, 2018.

688 Smith, A., Lott, N., and Vose, R.: *The Integrated Surface Database Recent
689 Developments and Partnerships*, *B Am Meteorol Soc*, 92, 704-708, 2011.

690 Sun, Y. L., Wang, Z. F., Dong, H. B., Yang, T., Li, J., Pan, X. L., Chen, P., and Jayne,
691 J. T.: Characterization of summer organic and inorganic aerosols in Beijing,
692 China with an Aerosol Chemical Speciation Monitor, *Atmos Environ*, 51, 250-
693 259, 2012.

694 Tsimpidi, A. P., Karydis, V. A., and Pandis, S. N.: Response of Fine Particulate
695 Matter to Emission Changes of Oxides of Nitrogen and-Anthropogenic Volatile
696 Organic Compounds in the Eastern United States, *J Air Waste Manage*, 58,
697 1463-1473, 2008.

698 Wang, G. H., Zhang, R. Y., Gomez, M. E., Yang, L. X., Zamora, M. L., Hu, M., Lin,
699 Y., Peng, J. F., Guo, S., Meng, J. J., Li, J. J., Cheng, C. L., Hu, T. F., Ren, Y. Q.,
700 Wang, Y. S., Gao, J., Cao, J. J., An, Z. S., Zhou, W. J., Li, G. H., Wang, J. Y.,
701 Tian, P. F., Marrero-Ortiz, W., Secret, J., Du, Z. F., Zheng, J., Shang, D. J.,
702 Zeng, L. M., Shao, M., Wang, W. G., Huang, Y., Wang, Y., Zhu, Y. J., Li, Y. X.,
703 Hu, J. X., Pan, B., Cai, L., Cheng, Y. T., Ji, Y. M., Zhang, F., Rosenfeld, D., Liss,
704 P. S., Duce, R. A., Kolb, C. E., and Molina, M. J.: Persistent sulfate formation
705 from London Fog to Chinese haze, *P Natl Acad Sci USA*, 113, 13630-13635,
706 2016.

707 Wang, H. C., Lu, K. D., Chen, X. R., Zhu, Q. D., Chen, Q., Guo, S., Jiang, M. Q., Li,
708 X., Shang, D. J., Tan, Z. F., Wu, Y. S., Wu, Z. J., Zou, Q., Zheng, Y., Zeng, L.
709 M., Zhu, T., Hu, M., and Zhang, Y. H.: High N₂O₅ Concentrations Observed in
710 Urban Beijing: Implications of a Large Nitrate Formation Pathway, *Environ Sci*
711 *Tech Let*, 4, 416-420, 2017a.

712 Wang, J. D., Zhao, B., Wang, S. X., Yang, F. M., Xing, J., Morawska, L., Ding, A. J.,
713 Kulmala, M., Kerminen, V. M., Kujansuu, J., Wang, Z. F., Ding, D. A., Zhang,
714 X. Y., Wang, H. B., Tian, M., Petaja, T., Jiang, J. K., and Hao, J. M.: Particulate
715 matter pollution over China and the effects of control policies, *Sci Total Environ*,
716 584, 426-447, 2017b.

717 Wang, S. X., Xing, J., Zhao, B., Jang, C., and Hao, J. M.: Effectiveness of national air
718 pollution control policies on the air quality in metropolitan areas of China, *J*
719 *Environ Sci*, 26, 13-22, 2014.

720 Wang, X. F., Wang, W. X., Yang, L. X., Gao, X. M., Nie, W., Yu, Y. C., Xu, P. J.,
721 Zhou, Y., and Wang, Z.: The secondary formation of inorganic aerosols in the

722 droplet mode through heterogeneous aqueous reactions under haze conditions,
723 *Atmos Environ*, 63, 68-76, 2012.

724 Wang, Y., Zhang, Q. Q., He, K., Zhang, Q., and Chai, L.: Sulfate-nitrate-ammonium
725 aerosols over China: response to 2000-2015 emission changes of sulfur dioxide,
726 nitrogen oxides, and ammonia, *Atmos Chem Phys*, 13, 2635-2652, 2013.

727 Wang, Y. L., Song, W., Yang, W., Sun, X. C., Tong, Y. D., Wang, X. M., Liu, C. Q.,
728 Bai, Z. P., and Liu, X. Y.: Influences of Atmospheric Pollution on the
729 Contributions of Major Oxidation Pathways to PM_{2.5} Nitrate Formation in
730 Beijing, *J Geophys Res-Atmos*, 124, 4174-4185, 2019.

731 Wen, L., Xue, L. K., Wang, X. F., Xu, C. H., Chen, T. S., Yang, L. X., Wang, T.,
732 Zhang, Q. Z., and Wang, W. X.: Summertime fine particulate nitrate pollution in
733 the North China Plain: increasing trends, formation mechanisms and implications
734 for control policy, *Atmos Chem Phys*, 18, 11261-11275, 2018.

735 Wen, Z., Xu, W., Pan, X. Y., Han, M. J., Wang, C., Benedict, K., Tang, A. H., Collet,
736 J. L., and Liu, X. J.: Effects of reactive nitrogen gases on the aerosol formation
737 in Beijing from late autumn to early spring, *Environ Res Lett*, 16, 025005, doi:
738 10.1088/1748-9326/abd973, 2021.

739 Womack, C. C., McDuffie, E. E., Edwards, P. M., Bares, R., de Gouw, J. A.,
740 Docherty, K. S., Dube, W. P., Fibiger, D. L., Franchin, A., Gilman, J. B.,
741 Goldberger, L., Lee, B. H., Lin, J. C., Lone, R., Middlebrook, A. M., Millet, D.
742 B., Moravek, A., Murphy, J. G., Quinn, P. K., Riedel, T. P., Roberts, J. M.,
743 Thornton, J. A., Valin, L. C., Veres, P. R., Whitehill, A. R., Wild, R. J., Warneke,
744 C., Yuan, B., Baasandorj, M., and Brown, S. S.: An Odd Oxygen Framework for
745 Wintertime Ammonium Nitrate Aerosol Pollution in Urban Areas: NO_x and
746 VOC Control as Mitigation Strategies, *Geophys Res Lett*, 46, 4971-4979, 2019.

747 Xie, M., Zhu, K. G., Wang, T. J., Yang, H. M., Zhuang, B. L., Li, S., Li, M. G., Zhu,
748 X. S., and Ouyang, Y.: Application of photochemical indicators to evaluate
749 ozone nonlinear chemistry and pollution control countermeasure in China,
750 *Atmos Environ*, 99, 466-473, 2014.

751 Xue, J., Yuan, Z. B., Lau, A. K. H., and Yu, J. Z.: Insights into factors affecting
752 nitrate in PM_{2.5} in a polluted high NO_x environment through hourly

753 observations and size distribution measurements, *J Geophys Res-Atmos*, 119,
754 4888-4902, 2014.

755 Xue, J., Yuan, Z. B., Griffith, S. M., Yu, X., Lau, A. K. H., and Yu, J. Z.: Sulfate
756 Formation Enhanced by a Cocktail of High NO_x, SO₂, Particulate Matter, and
757 Droplet pH during Haze-Fog Events in Megacities in China: An Observation-
758 Based Modeling Investigation, *Environ Sci Technol*, 50, 7325-7334, 2016.

759 Zaveri, R. A. and Peters, L. K.: A new lumped structure photochemical mechanism
760 for large-scale applications, *J Geophys Res-Atmos*, 104, 30387-30415, 1999.

761 Zaveri, R. A., Easter, R. C., Fast, J. D., and Peters, L. K.: Model for Simulating
762 Aerosol Interactions and Chemistry (MOSAIC), *J Geophys Res-Atmos*, 113,
763 D13204, doi: 10.1029/2007jd008782, 2008.

764 Zhai, S. X., Jacob, D. J., Wang, X., Shen, L., Li, K., Zhang, Y. Z., Gui, K., Zhao, T.
765 L., and Liao, H.: Fine particulate matter (PM_{2.5}) trends in China, 2013-2018:
766 separating contributions from anthropogenic emissions and meteorology, *Atmos*
767 *Chem Phys*, 19, 11031-11041, 2019.

768 Zhang, W. Q., Tong, S. R., Ge, M. F., An, J. L., Shi, Z. B., Hou, S. Q., Xia, K. H., Qu,
769 Y., Zhang, H. X., Chu, B. W., Sun, Y. L., and He, H.: Variations and sources of
770 nitrous acid (HONO) during a severe pollution episode in Beijing in winter 2016,
771 *Sci Total Environ*, 648, 253-262, 2019.

772 Zhang, Y. M., Wang, Y. Q., Zhang, X. Y., Shen, X. J., Sun, J. Y., Wu, L. Y., Zhang,
773 Z. X., and Che, H. C.: Chemical Components, Variation, and Source
774 Identification of PM₁ during the Heavy Air Pollution Episodes in Beijing in
775 December 2016, *J Meteorol Res-Prc*, 32, 1-13, 2018.

776 Zhao, M. F., Xiu, G. L., Qiao, T., Li, Y. L., and Yu, J. Z.: Characteristics of Haze
777 Pollution Episodes and Analysis of a Typical Winter Haze Process in Shanghai,
778 *Aerosol Air Qual Res*, 16, 1625-1637, 2016.

779 Zhao, P. S., Dong, F., He, D., Zhao, X. J., Zhang, X. L., Zhang, W. Z., Yao, Q., and
780 Liu, H. Y.: Characteristics of concentrations and chemical compositions for
781 PM_{2.5} in the region of Beijing, Tianjin, and Hebei, China, *Atmos Chem Phys*,
782 13, 4631-4644, 2013.

783 Zheng, B., Tong, D., Li, M., Liu, F., Hong, C. P., Geng, G. N., Li, H. Y., Li, X., Peng,
784 L. Q., Qi, J., Yan, L., Zhang, Y. X., Zhao, H. Y., Zheng, Y. X., He, K. B., and
785 Zhang, Q.: Trends in China's anthropogenic emissions since 2010 as the
786 consequence of clean air actions, *Atmos Chem Phys*, 18, 14095-14111, 2018.

787

788

Table 1. The emission scenarios in WRF-Chem numerical experiments

Simulation scenarios	Descriptions
B0	Base simulation under the 2016 emission conditions.
C_N ($N=1/2/\dots/8$)	Same as B0, but anthropogenic NO_x emissions are reduced by 10%, 20%...80%, respectively, relative to the usual levels in 2016.
C_{S-N} ($N=2/4/6/8$)	Same as B0, but anthropogenic SO_2 emissions are reduced by 20%, 40%...80%, respectively, relative to the usual levels in 2016.
C_{N-N} ($N=2/4/6/8$)	Same as B0, but anthropogenic NH_3 emissions are reduced by 20%, 40%...80%, respectively, relative to the usual levels in 2016.
C_{V-N} ($N=2/4/6/8$)	Same as B0, but anthropogenic VOC_s emissions are reduced by 20%, 40%...80%, respectively, relative to the usual levels in 2016.
NO	Same as B0, but only consider the NO_2+OH gas-phase oxidation pathway for the production of nitrate aerosol.
E1	Same as B0, but anthropogenic NO_x emissions are replaced using the MEIC inventory in 2012.

789

790

Table 2. Statistical evaluations of the model meteorological performance

Variable	Obs	Sim	R^a	MB ^a	NMB ^a	ME ^a	RMSE ^a
Period I (15 August to 16 September)							
Temperature ($^{\circ}\text{C}$)	24.04	23.91	0.89	-0.13	-0.55%	1.98	2.63
Humidity (%)	70.89	66.88	0.78	-4.01	-5.65%	11.07	14.67
Wind speed (m s^{-1})	2.46	3.04	0.50	0.58	23.72%	1.38	1.83
Period II (24 November to 26 December)							
Temperature ($^{\circ}\text{C}$)	3.43	3.40	0.94	-0.03	-0.80%	2.18	2.83
Humidity (%)	69.85	65.27	0.63	-4.58	-6.56%	13.51	17.88
Wind speed (m s^{-1})	2.61	3.66	0.55	1.06	40.64%	1.70	2.23

791

^a R : correlation efficient; MB: mean bias; NMB: normalized mean bias; ME: mean

792

error; RMSE: root mean square error.

793

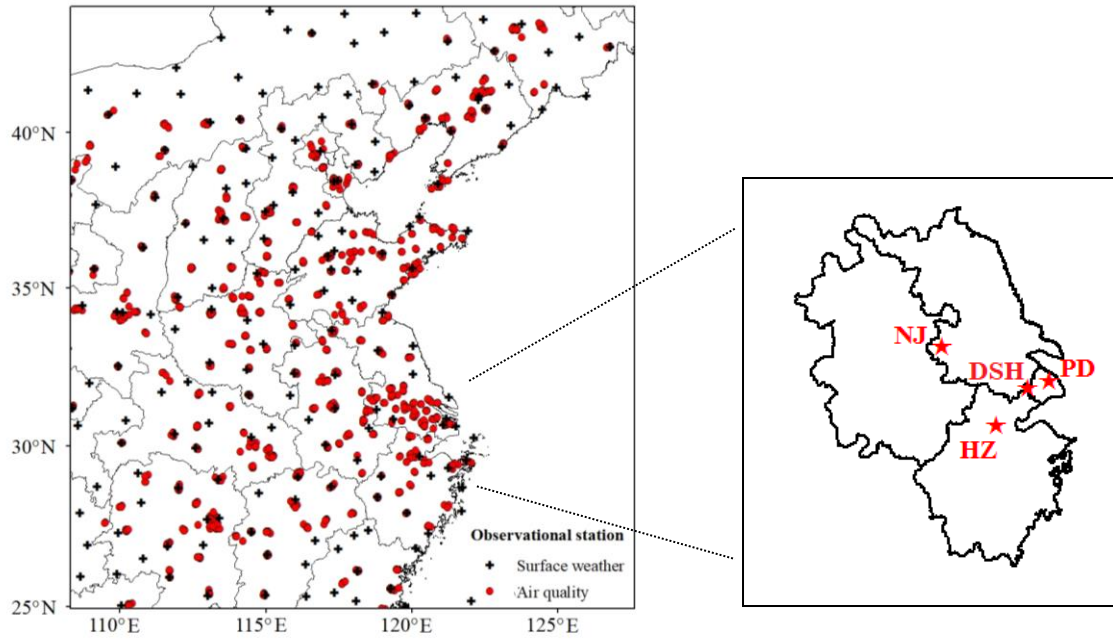
794

795

Table 3. Statistical evaluations of the model chemical performance

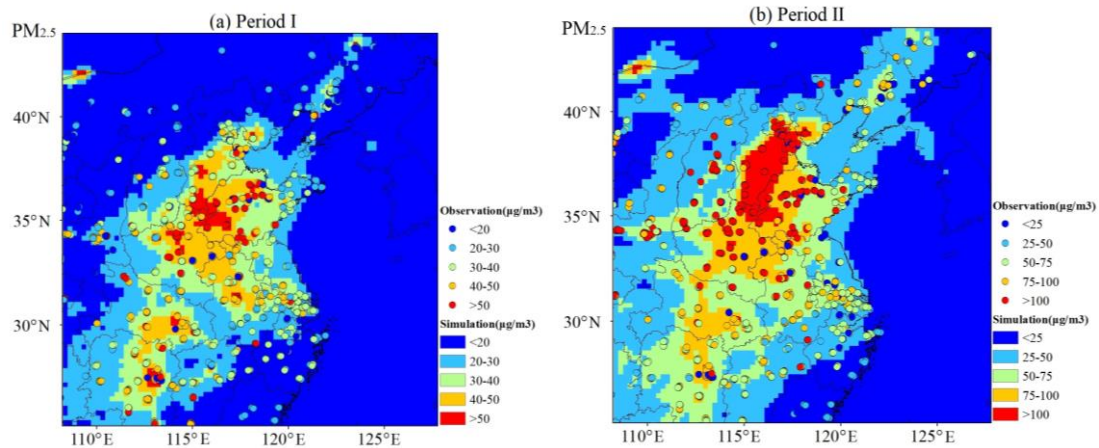
Variable	Obs	Sim	MB	NMB	Obs	Sim	MB	NMB
	Period I				Period II			
PM _{2.5}	36.88	33.22	-3.66	-9.92%	91.59	64.28	-27.31	-29.82%
SO ₂	17.65	16.51	-1.14	-6.46%	41.45	29.80	-11.65	-28.11%
NO ₂	28.53	33.23	4.70	16.47%	53.01	54.28	1.27	2.40%
Daily- maximum O ₃	237.45	255.77	18.32	7.72%	125.62	86.61	-39.01	-31.05%

796

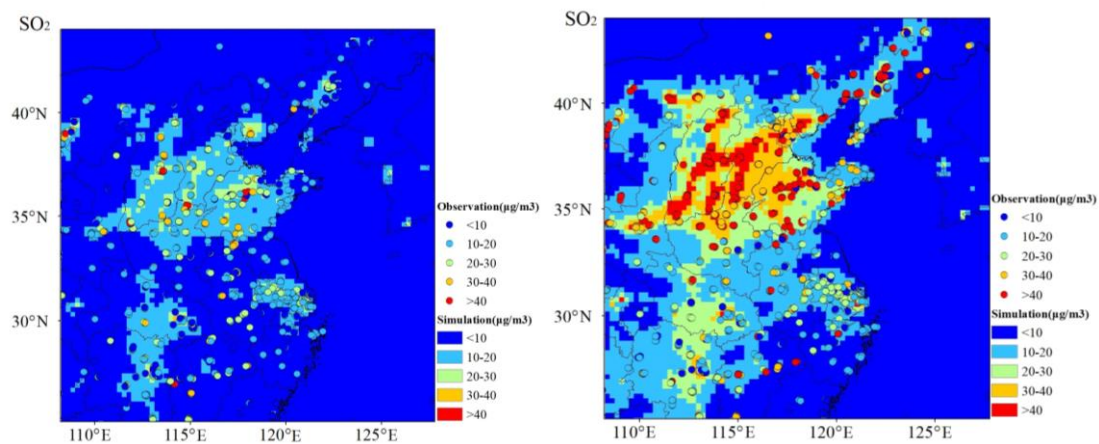


797 **Fig. 1.** WRF-Chem domain configuration and observational stations. Black crosses:
 798 surface weather stations; Red dots: CNEMC routine air quality monitoring stations;
 799 Red stars: surface supersites in YRD.

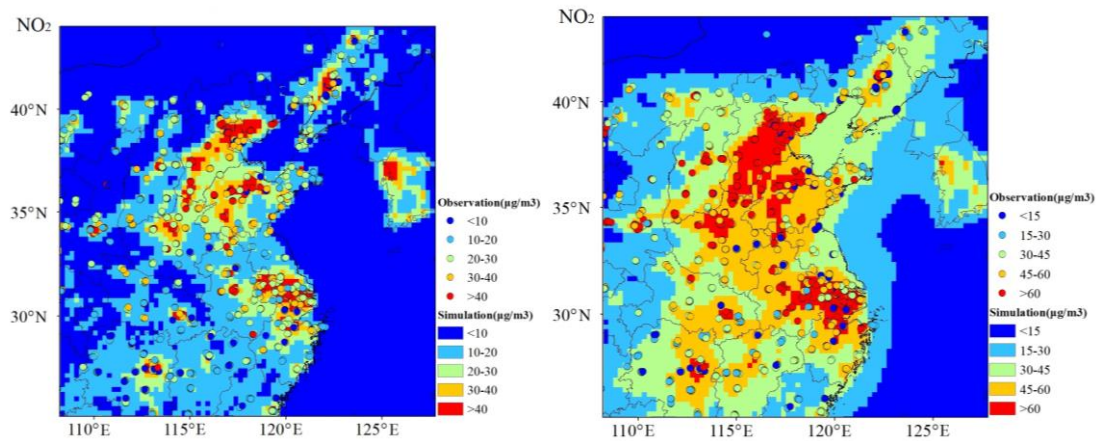
800



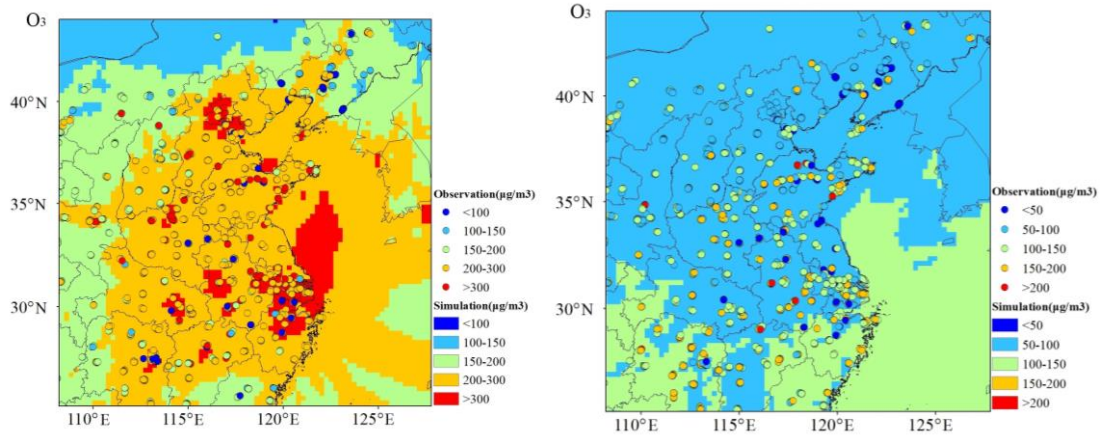
801



802



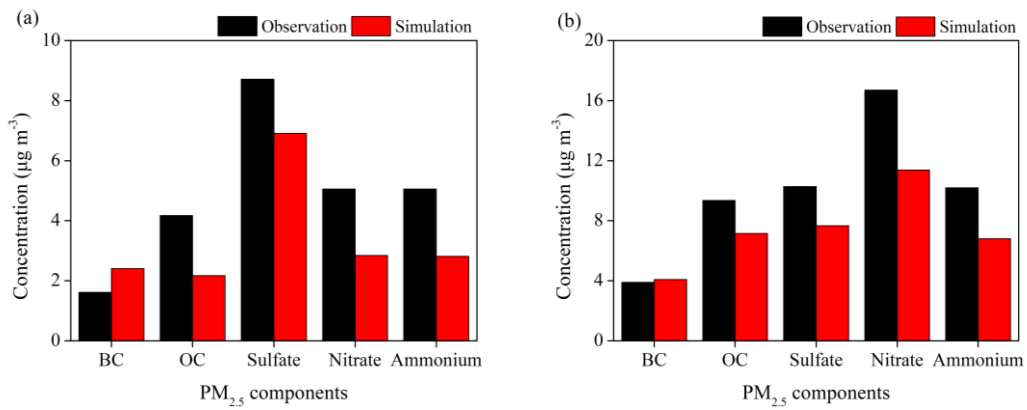
803 **Fig. 2.** Spatial patterns of the surface average PM_{2.5}, NO₂, SO₂ and daily-maximum
804 O₃ concentrations in Period I (left panels) and Period II (right panels) from the WRF-
805 Chem modeling (shaded contours) and routine air quality observations (dots).



806

807

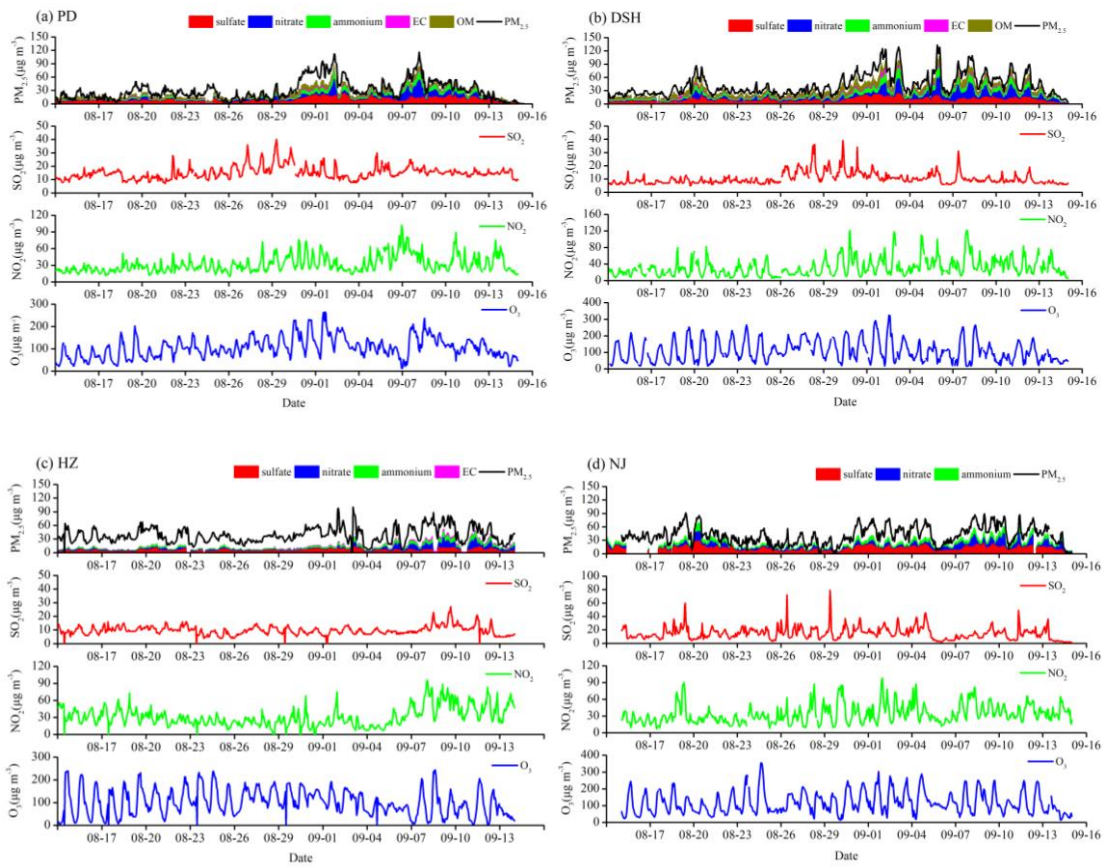
Fig. 2. Continued.



808

809 **Fig. 3.** Comparisons of surface PM_{2.5} components from WRF-Chem simulations and
 810 observations in Period I (a) and Period II (b) at the four supersites in YRD.

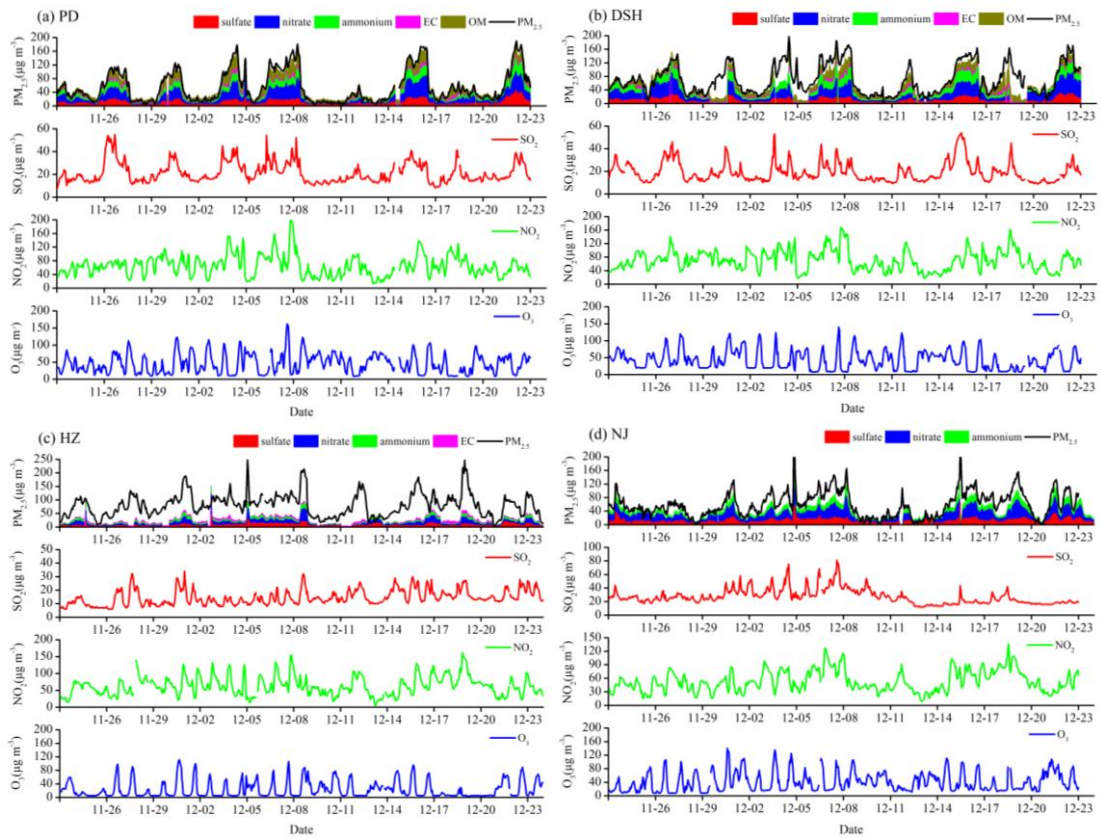
811



812

813

814 **Fig. 4.** Observed aerosol composition and gaseous pollutants concentrations at the
 815 four supersites during Period I.



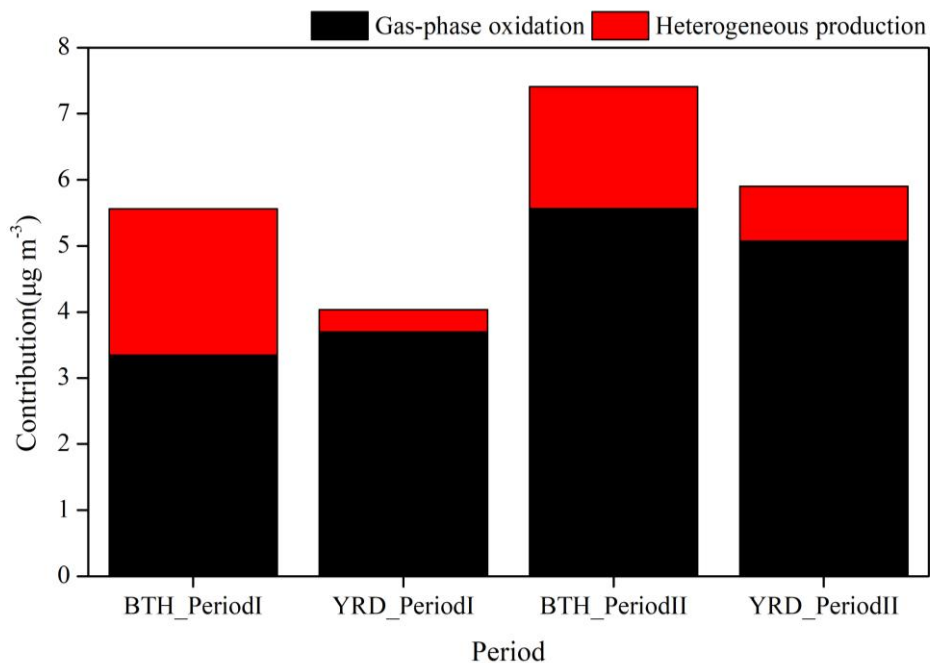
816

817

818

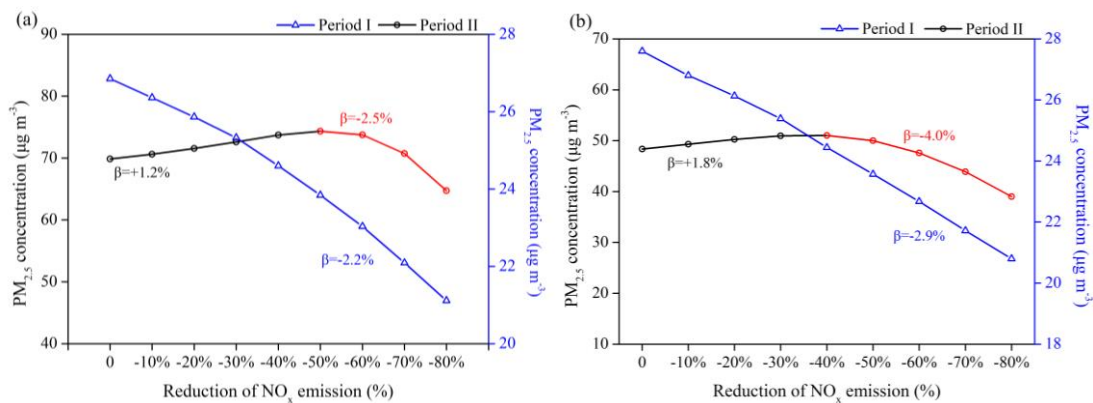
Fig. 5. Same as Fig. 4, but for Period II.

819



820

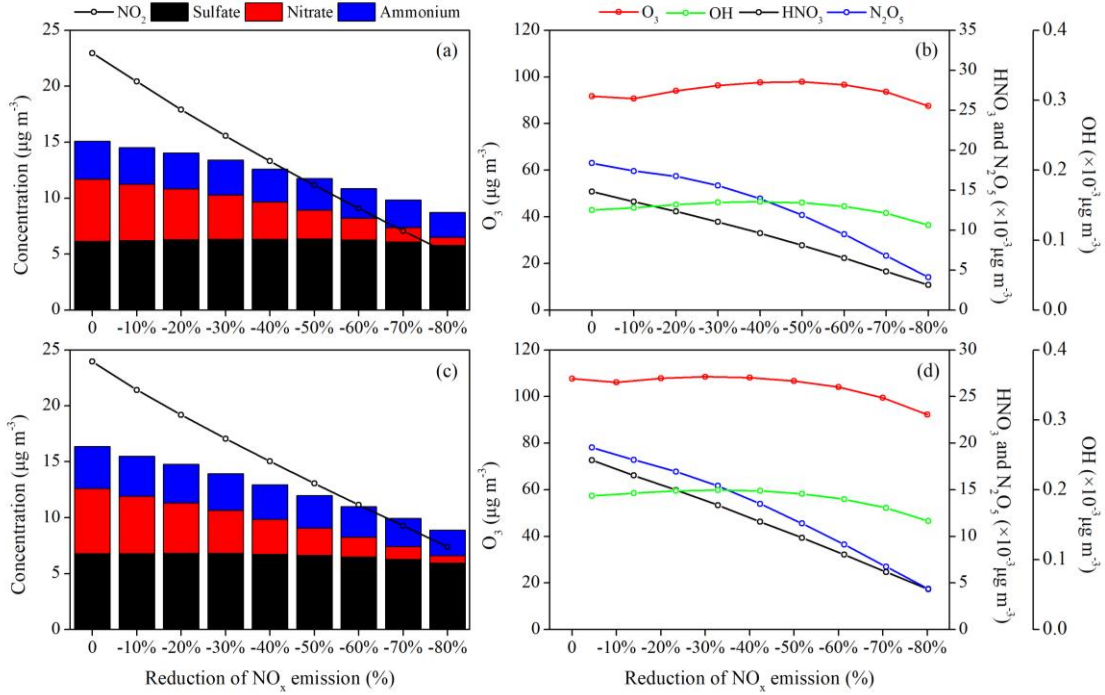
821 **Fig. 6.** Contributions of gas-phase oxidation and heterogeneous production to the
822 surface nitrate concentrations for the BTH and YRD regions in two seasons.



823

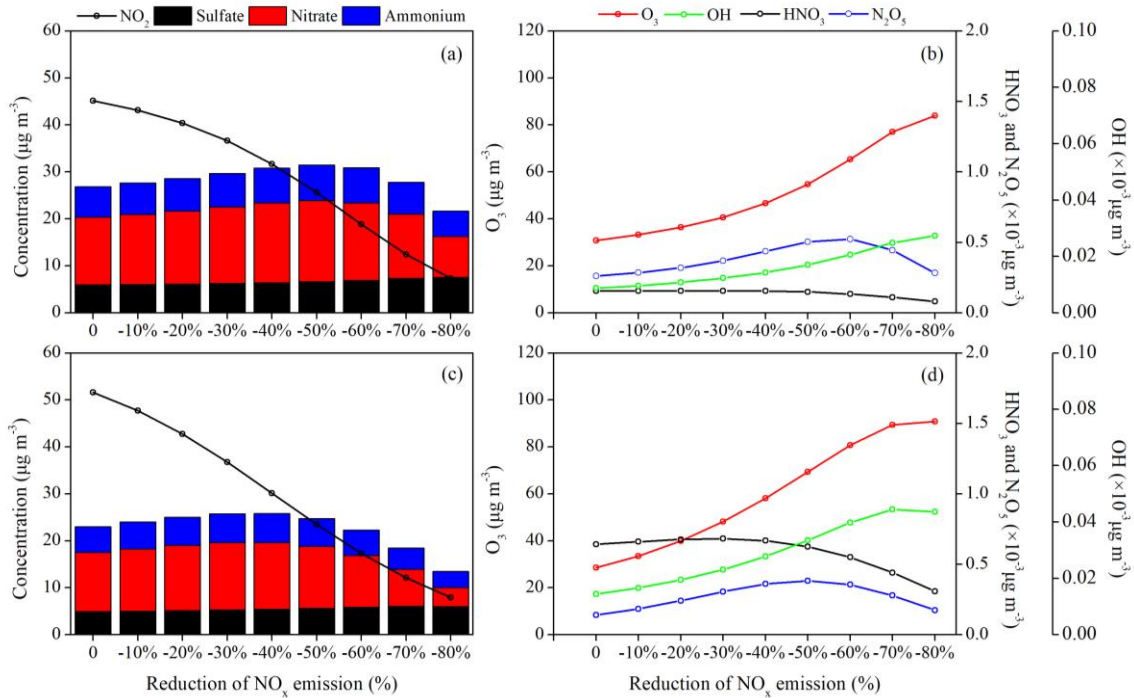
824 **Fig. 7.** Responses of surface PM_{2.5} concentrations to the NO_x emission reduction
825 scenarios in (a) BTH and (b) YRD. The calculated NO_x emission control efficiency (β)
826 is also marked in the figure.

827



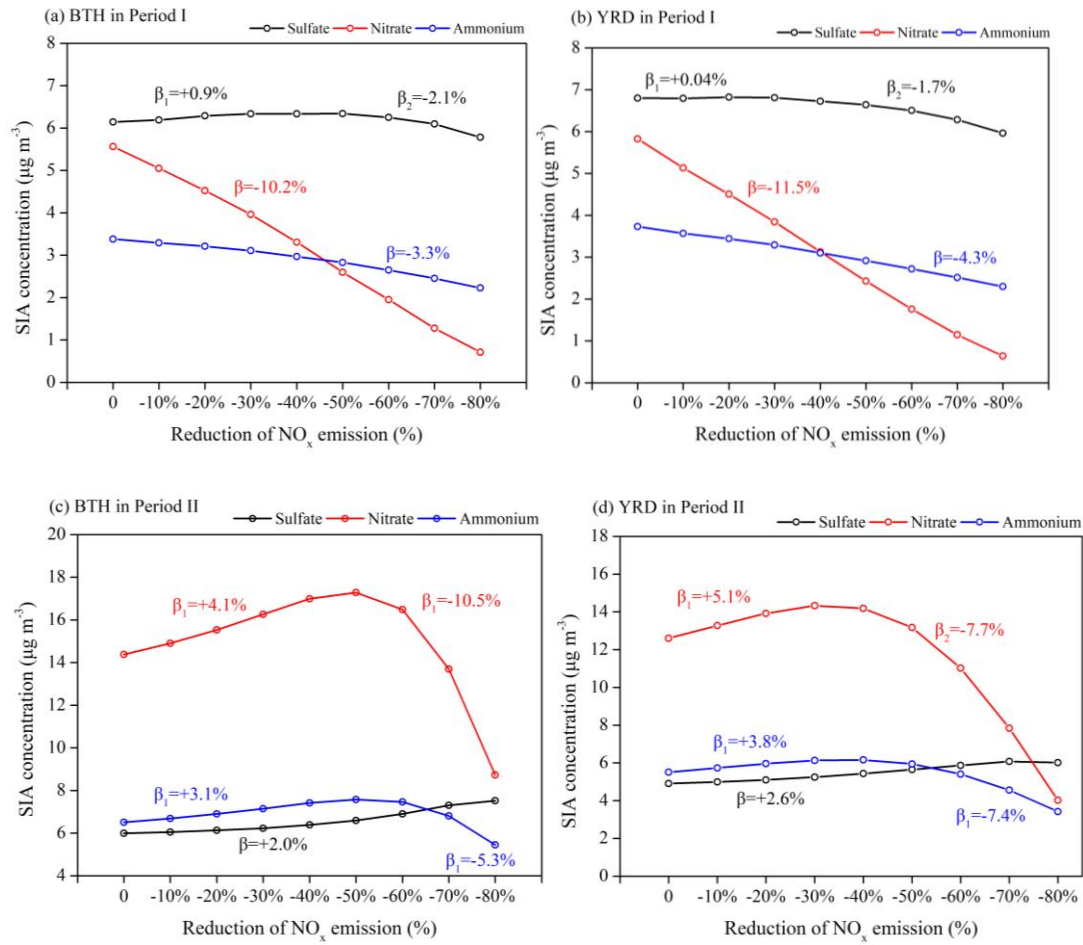
829

830 **Fig. 8.** Responses of the surface concentrations of SIA components and key
 831 atmospheric trace gases (NO₂, O₃, OH, HNO₃ and NO₃) to the NO_x emission
 832 reduction scenarios in (a, b) BTH and (c, d) YRD during Period I.



833
 834

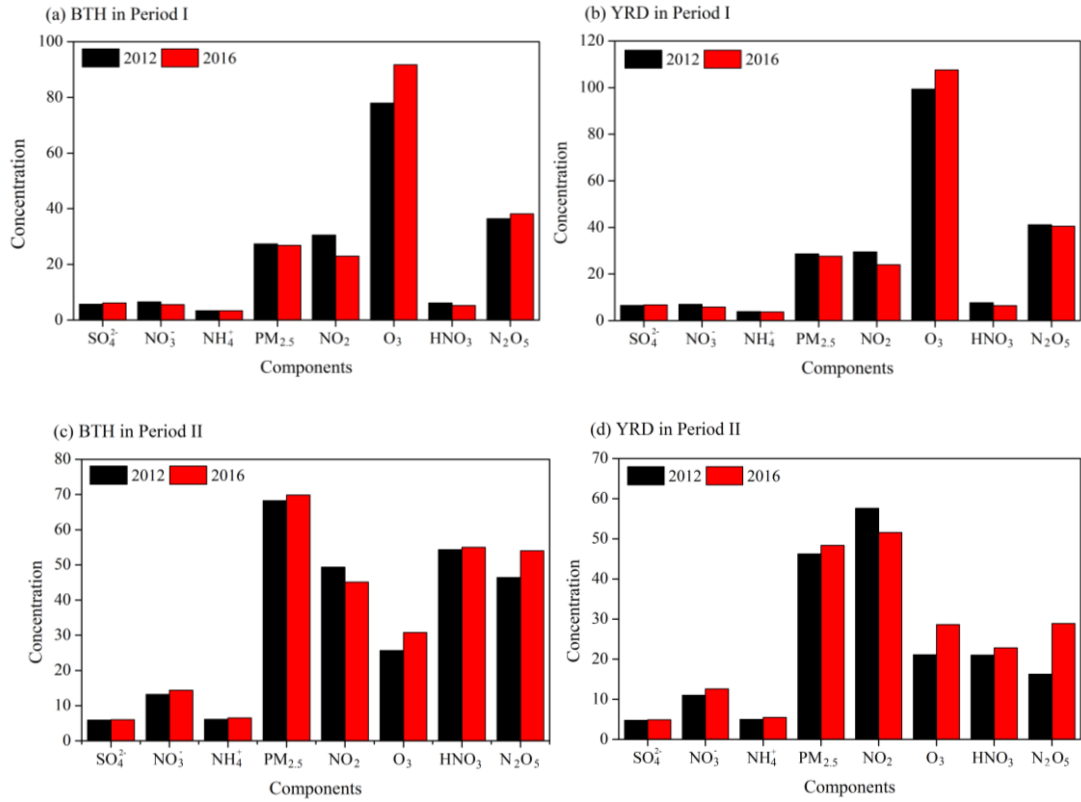
Fig. 9. Same as Fig. 8, but for Period II.



835

836

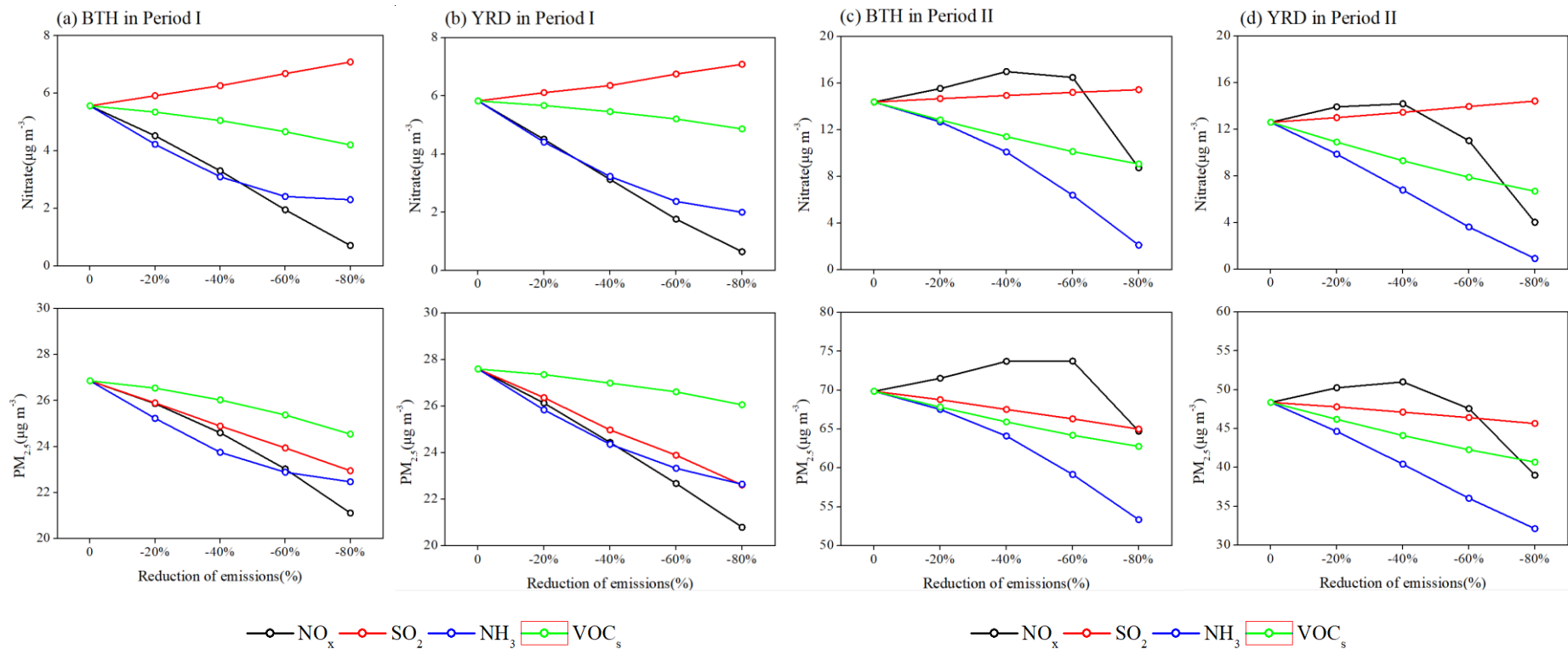
837 **Fig. 10.** Responses of the surface concentrations of SIA components to the NO_x
 838 emission reduction scenarios and their emission control efficiencies in (a, b) Period I
 839 and (c, d) Period II.



840

841

842 **Fig. 11.** Changes in the concentrations of surface $\text{PM}_{2.5}$, SIA components and key
 843 atmospheric trace (NO_2 , O_3 , HNO_3 and N_2O_5) due to the 2012–2016 NO_x emission
 844 reductions in China estimated as the differences between the base simulation and E1
 845 scenario. The units are ppt for HNO_3 and N_2O_5 , and $\mu\text{g m}^{-3}$ for other chemical species.



846

847

848 **Fig. 12.** Responses of the surface nitrate (upper panels) and $\text{PM}_{2.5}$ (bottom panels) concentrations to the emission reduction scenarios of NO_x ,
 849 SO_2 , NH_3 and VOC_s during Period I (a, b) and Period II (c, d).